MODELLING SIFRIM-HITZ-WEISS SYNDROME USING MOUSE GENETICS

SARAH LARRIGAN

Thesis submitted to the University of Ottawa
in partial Fulfillment of the requirements for the
Master's degree in Neuroscience

Department of Cellular and Molecular Medicine
Faculty of Medicine
University of Ottawa

Abstract

Neurodevelopmental disorders encompass a spectrum of different conditions with both genetic and environmental etiologies. Although rapid progress has been made in deciphering the genetic landscape of these disorders, in most cases, it remains unclear how mutations undermine neurodevelopmental mechanisms. However, increasing identification of risk genes suggests chromatin remodelling is frequently impacted. For instance, *de novo* variants encoding the chromatin remodeller CHD4 causes Sifrim-Hitz-Weiss syndrome, which manifests as an overgrowth-intellectual disability syndrome. To further understand *Chd4*'s role during cortical development, we excised the ATPase domain of *Chd4* in the germline or specifically in the developing telencephalon, creating three mouse models. Germline heterozygotes presented a slight decrease in brain weight, cortex area and Ctip2+ cells, with females displaying more overt impairments in learning and memory. Telencephalon-specific conditional heterozygotes exhibited slight changes in white matter, increased repetitive movements and altered social behaviours. Telencephalon-specific conditional knockouts presented with decreased brain size, brain weight, and cortex thickness due to decreased upper layer neurons, and anxiety phenotypes. These data reveal an unexpected complexity in the impacts of *Chd4* mutations on neurodevelopmental processes and behaviour.

Table of Contents

List of Tables

List of Figures

List of Abbreviations

ADNP	Activity-dependent neuroprotective protein
ADP	Adenosine 5′-triphosphate
ANOVA	Analysis of variance
ASD	Autism spectrum disorder
ATAC	Assay for Transposase-Accessible Chromatin
ATRX	Alpha-thalassemia/mental retardation
CHD	Chromodomain helicase DNA binding
CHDNT	N-terminal domain of CHD
CMV	Human cytomegalovirus
CNV	Copy number variations
DMS-5	Diagnostic and Statistical Manual of Mental Disorders fifth edition
DNA	Deoxyribonucleic acid
DUF	Domains of unknown function
EMX1	Empty Spiracles Homeobox 1
GATAD2A	GATA Zinc Finger Domain Containing 2A
GATAD2B	GATA Zinc Finger Domain Containing 2B
HDAC	Histone deacetylases

ID	Intellectual disability
INO80	Inositol requiring 80
ISWI	Imitation SWI
MBD	Methyl-CpG-binding domain
MRI	Magnetic resonance imaging
mRNA	Messenger RNA
MTA	Metastasis associated proteins
NDD	Neurodevelopmental disorder
NPC	Neural progenitor cell
NuRD	Nucleosome remodeling and deacetylase
OCT	Optimal cutting temperature
OGID	Overgrowth-intellectual disability
PBS	Phosphate-buffered saline
PCR	Polymerase chain reaction
PFA	Paraformaldehyde
PHD	Plant homeodomains
RBBP	retinoblastoma binding proteins
RNA	Ribonucleic acid

RNAi	RNA interference
SANT	Swi3, Ada2, N-Cor, and TFIIIB
SIHIWES	Sifrim-Hitz-Weiss syndrome
SNF2	Sucrose nonfermenting 2
SWI/SNF	Switching defective/sucrose non-fermenting
SWRI	SWI2/SNF2-Related 1

Acknowledgements

I am extremely grateful to my supervisor, Dr. Pierre Mattar, for welcoming me into his lab and providing his endless support and encouragement throughout this project. He created a wonderful environment in the lab where that felt exciting for scientists at all stages. Thank you as well to all current and previous lab members – your support – technical and moral – made this project one I was able to enjoy the process of a whole lot more.

Thank you as well to all my friends (new and old) and family as they supported me along this journey and were understanding of my irregular hours and delayed experiments. I couldn't have accomplished this (will all my sanity still intact) without you. Special mentions to Alexandra, Alex, Ashley, Beha, Kida, Kit, Laura, Lydia, Nasana, Sam, Shaima, Sujay, Suma, Vickey, and Wan-Li. I am so lucky to have you all in my life!

My thanks to the university for helping me navigate the complexities of being a graduate student, and the student counsel for providing extra community, support and resources. I also would like to thank the University of Ottawa Behaviour Core for their support and help during all hours of the week. Special thanks to Sarah Kealey and Katherine Tacay who helped run several of the behaviour tests and to Dr. Kerstin Ure for her guidance and advice. My thanks to Shrilaxmi Joshi and Sam Clémot-Dupont for their help with western blots and genotyping respectively. Thanks as well to my TAC members, Dr. Diane Lagace and Dr. David Picketts, for their advice and guidance as I completed this project, and who probably each saw me present as least thrice as much as is the minimum requirement per year. Thank you to the NSERC and the OGS agencies,

who supported me financially in this journey and through the especially challenging time of the pandemic.

And to everyone else I didn't get the chance to yet name, I thank you! This journey has been one of great personal and professional growth for me, and I leave feeling very enriched and grateful for every experience.

Chapter 1. Introduction

1.1 Neurodevelopmental Disorders

A recent study published that the prevalence of neurodevelopmental disorders (NDDs) represents at least 4.70% of the population, with even higher prevalence identified depending on study measures, study location and associated socio-contextual differences between locations[1]. Indeed, 5.1% of Canadians reported living with a developmental disability or disorder in 2017[2]. Moreover, it has been predicted that many individuals with NDDs are undiagnosed and that NDD prevalence may increase with improvements in diagnostic resources and healthcare access[1,3-9]. Despite this, our understanding of NDDs and development of effective treatments for individuals with NDDs is still limited.

The 5th Edition Diagnostic and Statistical Manual of Mental Disorders' (DSM-5; American Psychiatric Association, 2013) classification of NDDs includes intellectual disability (ID) disorders, communication disorders, autism spectrum disorder (ASD), attention-deficit/hyperactivity disorder, specific learning disorders, motor disorders and tic disorders, among others. Though each of these disorders has unique diagnosis criteria, in many cases they share overlapping symptoms. Conversely, individuals with the same diagnosis can exhibit great variance in terms of the symptoms they present with and/or the degree of severity of each symptom. Indeed, even within a given category of an NDD (e.g. ID, ASD), several different sub-classes have been identified, and can require unique customized treatments. Moreover, it is not uncommon for individuals to be diagnosed with multiple NDDs and/or additional neurological conditions including mental illnesses and psychiatric disorders, which can mask symptoms and further complicate diagnosis[10,11]. This can make it challenging to identify treatments that best

suit each person. For this reason, research that elucidates underlying mechanisms of NDDs and associated symptoms may allow this spectrum of disorders to be stratified, providing insight towards appropriately tailoring treatments to individuals.

Previously identified environmental factors causing NDDs include social deprivation, physical trauma, toxic substances, nutrition, and metabolic/infectious diseases[12]. An ever-increasing number of genetic risk factors have also been identified, including cases of chromosomal aberrations (e.g. Down Syndrome[13] and fragile X-syndrome[14])[15], copy number variations (CNVs)[16-18] and single nucleotide variants (including *de novo* variants)[19-32]. However, the majority of NDDs have no known cause. Research suggests that many of these unknown cases may be attributed to 1) many unique rare genetic variants that have a high impact on development and/or 2) individuals that have accumulated many variants (*de novo* and/or hereditary; SNV and CNVs) which culminate together to determine the severity and phenotype of a particular NDD[33]. This may help explain why specific mutations (seemingly identical CNVs, similar mutations in same gene etc.) do not always predict similar disease outcome, while mutations in different genes have been identified as the cause of indistinguishable patient phenotypes. Moreover, it can help explain how NDDs might have both a hereditary component, which has been implicated in twin studies[34], and a *de novo* component. Adding to this, research suggests that various identified causative genes converge on common cellular and biological processes, suggesting that diverse NDDs may share pathological mechanisms[19-21,25,26,29,35-37]. Hence, understanding how these common cellular pathways are affected across NDDs may provide new insights towards therapeutics and treatments targeted towards subsets of individuals with similarly affected processes. Based on the identities of identified risk genes, relevant

cellular pathways include synaptogenesis, cell proliferation, cell differentiation and chromatin remodeling. We sought to further investigate how chromatin remodelers affect neurodevelopment.

1.2 Chromatin Remodellers

The dynamic organization of DNA within the cell is critical for development and differentiation, and the nucleosome has been well established as playing a vital role in the organization process[38]. The nucleosome typically consists of 146bp of DNA wrapped around an octamer of H2A, H2B, H3 and H4 histones. The dynamic nature of chromatin is yielded in part by the various ways nucleosomes can be modified. Chromatin remodelling encompasses the various ways chromatin structure can be altered and controlled via histone-modifying enzymes. During neurodevelopment, chromatin remodelling helps orchestrate a range of important and complex processes including progenitor proliferation, neural migration, cell differentiation and synapse maturation. Chromatin remodelers contribute to this process by using energy derived from ATP-hydrolysis in order to mobilize and remodel nucleosomes[39-42]. This ability is endowed to them by an SNF2 (sucrose nonfermenting 2)-like ATPase domain, which can be subdivided into two linked RecA-like lobes (also denoted as DExx and HELICc) that are linked by a variable insertion. Chromatin remodelers are additionally classified into at least four different families dependent on the other functional domains they possess; the SWI/SNF (switching defective/sucrose non-fermenting) family; the ISWI (imitation SWI/SNF) family; the INO80 (inositol requiring 80) family; and the CHD (chromodomain helicase DNA binding) family. Additionally, several orphan families of chromatin remodellers have also been identified. This includes the ATRX (alpha-thalassemia/mental retardation) family and the SWRI (SWI2/SNF2-

Related 1) family[41,43]. The genes in these families are well-conserved across evolution. Chromatin remodellers also commonly form multisubunit complexes, including the nucleosome remodeling and deacetylase (NuRD) complex (CHD family, ~10 subunits) to facilitate and enhance remodelling activities[41]. Here we will focus on CHD4 of the CHD family.

1.3 The CHD family

The chromodomain helicase gene family encodes a class of ATP-dependent chromatin remodeling proteins, which can evict or slide nucleosomes in order to remodel the epigenetic state of target genes. As such, they have been implicated in a variety of processes including transcription, proliferation and genome integrity, as well as cancer, NDDs and other developmental disorders in humans[44]. A total of 10 distinct members (CHD1, CHD1L, CHD2-9) have been identified so far, which have been further classified into three subfamilies based on homologous protein domains. A SNF2-like ATP-dependent helicase motif and two tandem chromodomains (chromatin organization modifier domains) are found in all CHD proteins. Members of Subfamily I (CHD1/CHD2) have a DNA binding domain with preference for AT-rich sequences[45]. Members of Subfamily II (CHD3/CHD4/CHD5) have dual plant homeodomains (PHDs) which can interact with methylated histone residues and protein cofactors[46-51]. Lastly, members of Subfamily III (CHD6/CHD7/CHD8/CHD9) have BRK domains, a SANT-like domain, CR motifs and a non-sequence-specific DNA binding domain[44].

Interestingly, mutations in nearly all of the CHDs have been associated with neurodevelopmental disorders[52-55]. *CHD2* mutations have been implicated in autosomal dominant childhood-onset epileptic encephalopathy syndrome[56-58]. *CHD1*, *CHD3*, and *CHD4* mutations have been shown

to cause the dominantly inherited neurodevelopmental syndromes Pilarowski-Bjornsson syndrome[59], Snijders Blok-Campeau syndrome[60] and Sifrim-Hitz-Weiss syndrome[61-63] respectively, discussed further below. *CHD5* has been implicated in neuroblastoma[64], a cancer that develops from immature neural cells, and missense and truncation variants in *CHD5* have been linked to an autosomal dominant neurodevelopmental syndrome with ID, epilepsy and behavioural symptoms (Parenti-Mignot neurodevelopmental syndrome (PMNDS))[65]. Mutations in *CHD7* have been shown to cause CHARGE syndrome[66-69], characterized by a multitude of developmental features, with a large percentage of these patients reported to also have ASD-like behaviours[70]. Mutations in *CHD8* have been implicated in causing an overgrowth-intellectual disability (OGID) syndrome called Zahir Friedman syndrome, which is associated with microcephaly[71]. *CHD8* has also been identified as one of the most significant risk genes for ASD[24,37,72] and associated with schizophrenia[73]. Additionally, mutations in *CHD2*, *CHD6* and *CHD7* have been shown to cause rare cases of ASD, ID or epilepsy[24,74-77]. Furthermore, variants in other subunits of chromatin remodelling complexes have also been implicated in NDDs[27,78,79]. We will go into more depth on two of the CHD4-associated chromatin remodelling complexes below.

1.4 The NuRD complex & the ChAHP complex

CHD3, CHD4 and CHD5 are the only known CHDs to associate with the NuRD complex. This complex, also known as the Mi-2β complex, is highly conserved across plants and animals and regulates gene expression across multiple tissues[80-83]. It functions to remodel chromatin structure and has been accordingly implicated in a variety of important cellular processes, including neurogenesis and corticogenesis[84]. Outside of the brain, it has also been implicated in stem cell

differentiation, embryonic development, and genomic integrity[85-88]. The NuRD complex is often characterized by transcriptional repressor activity, however it has also been implicated in other transcriptional activities, including gene activation[88,89].

Six core subunits of the NuRD complex, all of which contain several paralogues, have been identified[90] (Figure 1.1). These are the chromodomain-helicase DNA-binding proteins (CHD3/CHD4/CHD5); the histone deacetylases (HDAC1/HDAC2); the metastasis associated proteins (MTA1/MTA2/MTA3); the GATA zinc finger domain proteins (GATAD2B/GATAD2A); the retinoblastoma binding proteins (RBBP4/RBBP7); and the methyl-domain binding proteins (MBD2/MBD3). It is thought that the histone deacetylase module is formed from two HDAC1/2 subunits, an MTA1/2/3 dimer, and four RBBP4/7 proteins. MBD2/3, in turn, is thought to connect the MTA1/2/3 dimer to an individual GATAD2A/B subunit, which recruits a single CHD3/4/5 subunit to form the chromatin remodelling module[90-94]. Moreover, it has been shown that the NuRD complex can be functionally specialized depending on which subunits it incorporates. For instance, during neurodevelopment, it has been shown that the sequential switching of the CHD3/CHD4/CHD5 homologues is required for transcription regulation of distinct aspects of embryonic cortical development[84]. Moreover, the NuRD complex has been shown to interact with transcription factors to further dictate how and where it regulates the genome, such as Ctip2 and Ikaros[95-98].

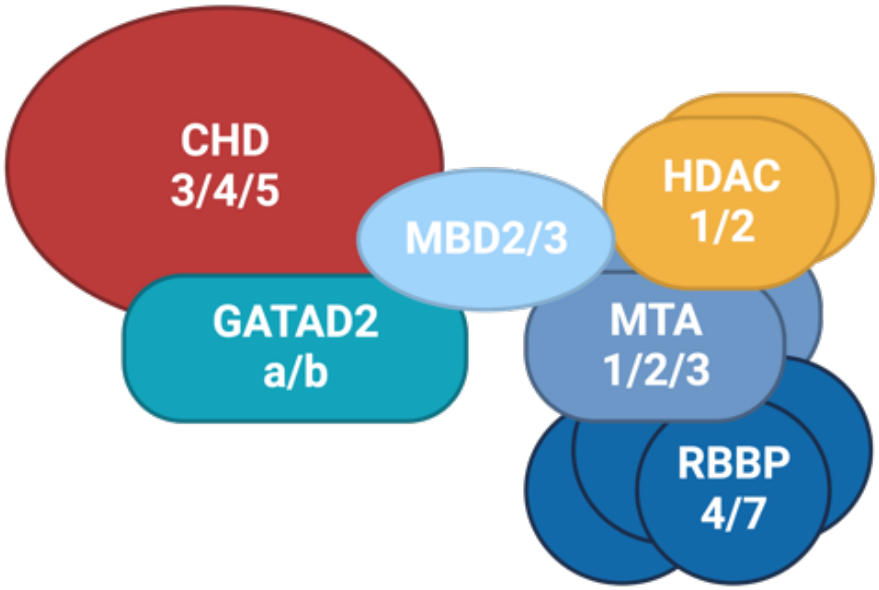

Figure 1.1. The NuRD Complex subunits. The NuRD complex encompasses 6 core subunits: the chromodomain-helicase DNA-binding proteins (CHD3/CHD4/CHD5), the GATA zinc finger domain proteins (GATAD2B/GATAD2A), the histone deacetylases (HDAC1/HDAC2), the methyl-domain binding proteins (MBD2/MBD3), the metastasis-associated proteins (MTA1/MTA2/MTA3), and the retinoblastoma binding proteins (RBBP4/RBBP7). Nucleosome remodeling and histone deacetylate activity are rendered by the CHD and HDAC units, respectively. The specific subunit homologues can confer functional specialization to the complex. Several of the subunits are also not exclusive to the NuRD complex. Created with BioRender.com.

From Larrigan et al. *International Journal of Molecular Sciences* (2021)

Several of the NuRD subunit genes have also been associated with neurodevelopmental disorders. *CHD3*, *CHD4* and *GATAD2B*-associated NDDs present as OGID syndromes with overlapping phenotype including microcephaly and ID, as well as motor/language delays, high forehead/frontal bossing, and enlarged cerebral spinal fluid spaces. Because of this, the term "NuRDopathies" has been proposed to further classify these OGID syndromes[54]. Interestingly, however, *CHD3* and *CHD4* syndromes also have distinct features, supporting the hypothesis that they play distinct roles during neurodevelopment[99]. Indeed, it has been shown these proteins also exhibit differences in their spatiotemporal expression patterns and functional specificity, as mentioned above[84]. More recently, as aforementioned, *CHD5* has also been implicated in an autosomal dominant neurodevelopmental syndrome with ID (PMNDS)[65]. Additionally, *MBD3* has been associated with ASD[79], and *CASZ1*, encoding another protein known to interact with the NuRD complex, has been associated with ID and ASD[100,101]. Future work might place these proteins under the umbrella of NuRDopathies as well, which might allow for further elucidation of the responsible molecular pathways.

CHD4 is also an important member of the ChAHP complex. Research so far suggests this complex is associated with gene repression and composed of Activity-dependent neuroprotective protein (ADNP), CHD4 and Heterochromatin protein 1 (HP1)[102]. Work in cultured cells suggests CHD3 and CHD5 may be able to incorporate in the ChAHP complex as well[103]. Notably, *ADNP* mutations also cause a neurodevelopmental syndrome known as Helsmoortel-Van Der Aa syndrome, and *ADNP* is one of the top risk genes associated with ASD[104]. We will focus more on the *CHD4*-associated syndrome below.

1.5 Sifrim-Hitz-Weiss syndrome

De novo variants in *CHD4* cause the OGID syndrome known as Sifrim-Hitz-Weiss syndrome (SIHIWES)[61-63]. The most recent study to date on this syndrome has identified a total of 32 individuals with this *CHD4* syndrome. All participants were heterozygous with nearly all pathogenic variants being missense or in-frame insertions/deletions, with the exception of three variants predicted to yield truncated proteins. Notably, the majority of the variants were found within the SNF2-like domain of *CHD4* - 16 individuals with C-terminal helicase variants and 6 individuals with N-terminal ATPase variants (Figure 1.2). Though the location of the variants did not appear to track or be associated with specific symptoms.

Mild to moderate ID (19/22 school aged participants), macrocephaly (11/28 participants), and speech delay (29/31 participants) were identified frequently in individuals. Additionally, of the 23 individuals that underwent brain imaging (MRI), 22 (96%) presented with various types of brain abnormalities including ventriculomegaly, hydrocephalus requiring shunting, Chiari 1, and a thin corpus callosum. Together, these findings highlight the neurodevelopmental aspects of this syndrome. Outside of the brain, this disorder is also associated with hearing loss, hypotonia, gross motor delays, and abnormalities in the heart, skeleton, and gonads. Additionally, a subset (3 participants) had growth hormone deficiency. These findings support the idea that *Chd4* acts in basic developmental processes.

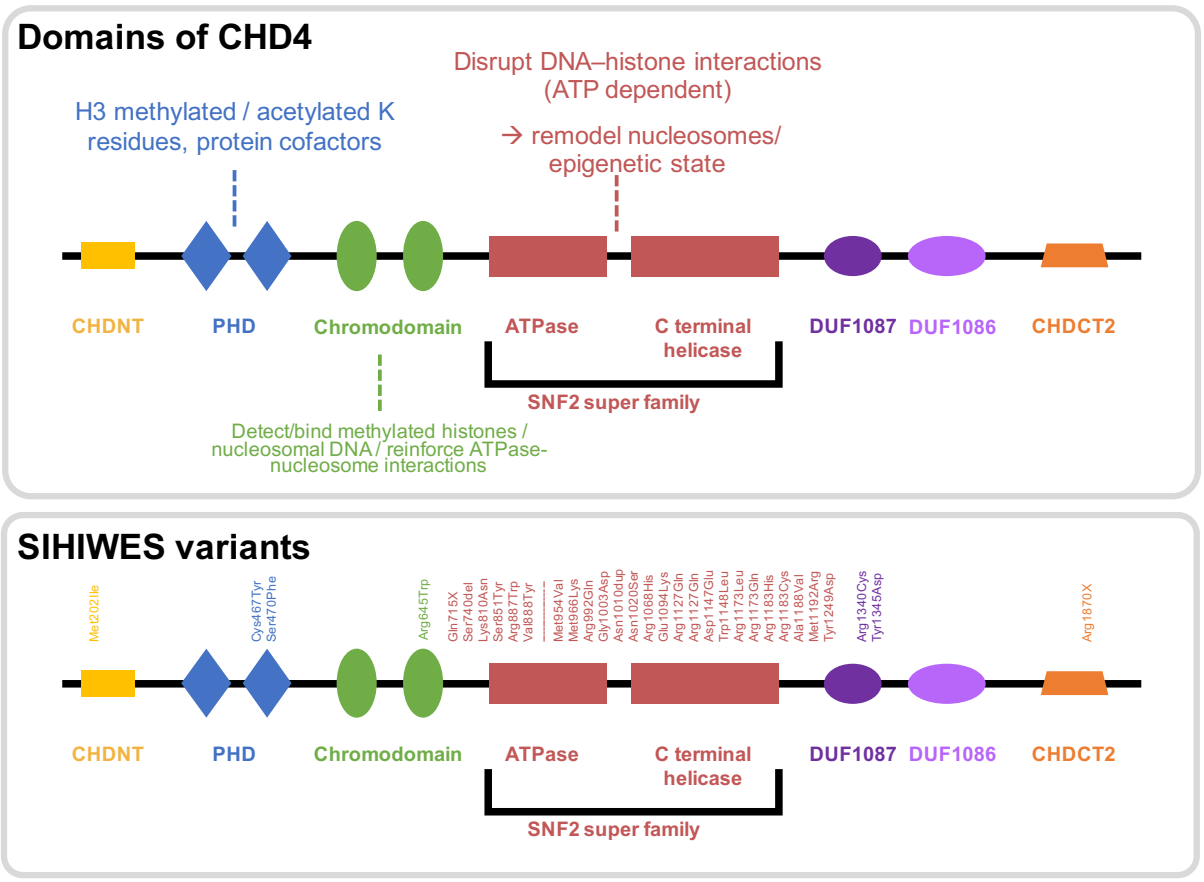

Figure 1.2. Domains of CHD4 and associated Sifrim-Hitz-Weiss syndrome variants. Top) The various domains of CHD4 and their associated roles including N-terminal domain of CHD (CHDNT), plant homeodomain (PHD), chromodomains, ATPase domain, C-terminal helicase domain, domains of unknown function (DUF1087, DUF1086) and CHDCT2 C-terminal domain. Bottom) Identified *Chd4* variants in Sifrim-Hitz-Weiss syndrome. Red line indicates separation between variants in the ATPase domain versus the C-terminal helicase domain.

Adapted from Weiss et al. *Genetics in Medicine* (2019)

Weiss et al. revealed that two of the missense mutations in the C-terminal helicase domain of *CHD4* did not appear to affect CHD4's ability to interact with HDAC or localize to the nucleus when transfected into HEK293 cells. This suggests these mutants might instead impair complex activity[63]. Further investigations revealed that most SIHIWES variants exhibited a decrease in ATP hydrolysis and chromatin remodelling activities compared to wildtype[62]. These data give clues toward how a small subset of *CHD4* variants may impact neurodevelopment, though more research is needed to understand how variants lead to changes in phenotype at an organism level.

1.6 Neurodevelopment in the cortex

The mature six-layered mammalian neocortex (cerebral cortex) is highly specialized and has been extensively studied due to its rapid evolution in mammals and expansion in humans. Many NDDs have been linked to impaired neocortical development[105]. At around E9.5, the neural tube gives rise to the telencephalon in the murine brain. The dorsal telencephalon goes on to develop the neocortex, as well as additional structures, including the olfactory cortex and hippocampus. The unique layered organization of excitatory neurons within the cortex is generated by progenitor cells between ~E11-E18[105,106] (Figure 1.3). Briefly, neuroepithelial cells within the ventricular zone proliferate and differentiate into radial glial cells (apical progenitors) between ~E10-E12. The radial glia undergo asymmetric divisions to generate deep layer neurons (~E11-E13), then upper layer neurons (~E14-E18), allowing for cortical neuron development in an inside out fashion. Some radial glial also generate intermediate progenitor cells (basal progenitors), which typically divide symmetrically into two daughter cells that tend to migrate to the upper layers. Hallmark transcription factors have been identified that help determine final neuron identity and discriminate between the various neural subtypes (Table 1). Following

neuron generation, radial glia progenitors switch to generating glial cells within the cortex (~E18 onwards)[107]. Cells created outside the cortex, including Cajal-Retzius cells, cortical interneurons, and the initial wave of oligodendrocyte precursors, also migrate tangentially into the cortex during the development process. Postnatally, neocortical development includes the generation of glial cells, layer maturation, and circuit refinement.

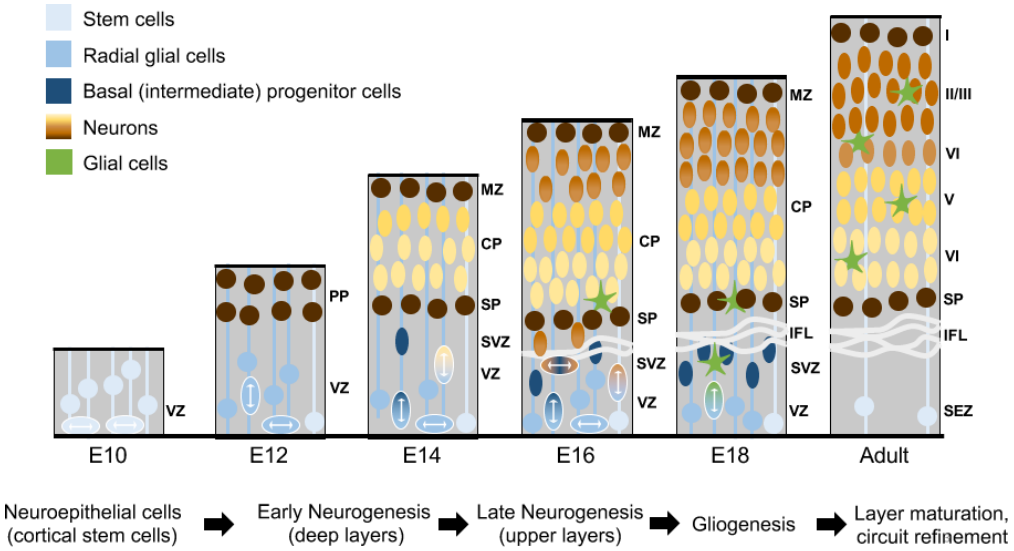

Figure 1.3. Development of the six-layered mouse neocortex. Neuroepithelial cells (very light blue) within the ventricular zone proliferate and differentiate into radial glial (light blue) progenitors between ~E10-E12. Radial glia undergo asymmetric divisions and generate cells that help form the preplate (PP; dark brown), which then splits into the marginal zone (MZ (also known as layer I)) and subplate (SP). The radial glia continue undergo asymmetric divisions to yield early-born deep layer V and VI neurons (yellow) and late-born upper layer IV and II/II neurons (brown), migrating into the cortical plate (CP) in an inside out fashion. Around E13, some radial glia cells also generate intermediate (basal) progenitor cells (dark blue), which typically divide into two daughter neurons that migrate to the upper layers. Radial glia progenitors then switch to generating glial cells (green). Cells created outside the cortex, including Cajal-Retzius cells, cortical interneurons, and the initial wave of oligodendrocyte precursors, also migrate tangentially into the cortex during the development process (not shown).

From Larrigan et al. *International Journal of Molecular Sciences* (2021)

Table 1. Cell specific markers in the murine cortex. Examples of markers expressed in neural and glial subtypes in the murine cortex.

Marker	~E10-E11 Start of Neurogenesis	~E13.5-E14.5 Transition from deep to upper layer neurogenesis	~E15-E17 Transition from neurogenesis to gliogenesis	~E18.5-P0 Birth	P7/Adult Mature neocortex
Pax6	Neural stem cells	Radial glia cells	Radial glia cells	Radial glia cells	-
Neurog2	Neural stem cells (subset)	Radial glia cells (subset)	Radial glia cells (subset)	Radial glia cells (subset)	-
Tbr2	Preplate neurons	Basal (intermediate) progenitor cells	Basal (intermediate) progenitor cells	Basal (intermediate) progenitor cells	-
Tbr1	-	Immature neurons/deep layer neurons	Immature neurons/deep layer neurons	Immature neurons/deep layer neurons	Deep layer neurons
Ctip2	Outer layers of cortex	Deep layers	Deep layers	Deep layers	Deep layers (V-VI)
Brn2	-	Upper layers	Upper layers	Upper layers	Upper layers (II-IV)
Gfap	-	-	-	Astrocytes	Astrocytes
Olig2	-	-	Oligodendrocytes progenitor cells	Oligodendrocytes	Oligodendrocytes

1.7 *Chd4* and neurodevelopment in rodents

Chd4 germline mutants are unable to implant, making them inviable and highlighting its role as an essential gene[108]. Moreover, even though mouse knockout model of exons 11 and 12 of the *Chd4* chromodomains did manage to implant, the knockouts were embryonic lethal prior to organogenesis (International Mouse Phenotyping Consortium (IMPC)). Conditional knockouts are thus important for studying Chd4's requirement in neurodevelopment. Indeed, research has implicated *Chd4* in various aspect of neurodevelopment including regulation of neurogenesis and neural plasticity in rodents[84,109-112]. In primary cortical cultures, *Chd4* was shown to suppress astroglial differentiation in neural progenitor cells (NPCs)[109]. The role of *Chd4* in the NuRD complex was also implicated during embryonic cortical development[84]. *Nestin-Cre* driven conditional knockout of *Chd4* in the embryonic nervous system resulted in reduced proliferation of apical NPCs and reduced number and proliferation of basal NPCs. This led to a decrease in cortical plate thickness – particularly in the upper layers (II and III), but not lower layers (IV-VI), of the cortex. This also contributed toward reduced brain size and cortical thickness in these

conditional knockouts. *Nestin-Cre Chd4* conditional knockouts were also perinatally lethal, further highlighting *Chd4*'s importance during neurodevelopment[4]. Conversely, it was shown that *Chd4* did not appear to have an effect on cortical radial migration or neuronal polarity, whereas these aspects were affected by *Chd3* and *Chd5* knockdown. Since CHD subunits are monomeric within NuRD, they incorporate into the complex in a mutually exclusive fashion[54]. Accordingly, it was shown that Chd3, Chd4 and Chd5 incorporated into the NuRD complex in a temporal fashion during cortical development. The form of the NuRD complex with Chd4 appears to be most prominent during the earlier stages of development (~E12.5) in the neural progenitor cells, while Chd3 and Chd5 appear to be expressed and incorporated into the complex at later stages of neurodevelopment when migrating neurons are more abundant. This temporal expression pattern appears to correlate with their non-overlapping roles during cortical development.

In addition to neurogenesis, *Chd4* may also contribute to the functions of postmitotic neurons. Conditional knockout of *Chd4* in cerebellar granule neurons of mice and knockdown of *Chd4* by RNAi in rats revealed that *Chd4* was required for proper development of synaptic connectivity in the cerebellar cortex[110]. Another study found that *Chd4* knockout in the granule neurons of the mouse cerebellum also impaired dendrite pruning, and that these mice exhibited deficits in procedural learning behaviour tests, such as the accelerating rotarod[111]. In both studies, these essential Chd4 functions were linked to the NuRD complex and transcriptional repression, since RNAi on other NuRD subunits phenocopied *Chd4* ablation. Additionally, it has been shown that *Chd4* knockout in murine postmitotic cerebellar granule neurons results in increased accessibility

to enhancers and promoters on a genome-wide basis, which had concomitant effects on gene expression[112].

1.8 Research Gaps in studying *Chd4*

Though previous research highlights a clear role for *Chd4* during neurodevelopment, the role of *Chd4* during cortical development remains to be fully elucidated. For instance, 1) research in the cerebellum suggests that *Chd4* may also play a role in post-mitotic neurons, which has yet to be addressed in the cortex. Moreover, 2) cortical development (encompassing neurogenesis, gliogenesis, layer specific cell differentiation, and cortical arealization) continues during the first postnatal week. However previous attempts to knockout *Chd4* in neural progenitors led to perinatal lethality, preventing examination beyond birth. Additionally, 3) a thorough investigation between *Chd4* function and behaviour has yet to be performed despite clear links of *Chd4* variants in humans with intellectual disability. This precludes our understanding of how changes in *Chd4* lead to clinically relevant phenotypes. 4) Previous work with *Chd4* knockout in NPCs resulted in a microcephaly phenotype resulting from impaired NPC proliferation and cell death. However, many individuals with *de novo Chd4* mutations present with macrocephaly, suggesting that *Chd4* might regulate uncharacterized aspects of neural progenitor proliferation not previously captured by knockout models. Lastly, 5) previous studies described phenotypes almost exclusively in *Chd4* knockouts, whereas *Chd4* syndrome is heterozygous in nature. Examining heterozygotes in more detail may help provide further insight into whether *Chd4* variants act in a loss-of-function or dominant-negative fashion in Sifrim-Hitz-Weiss syndrome. We aimed to expand upon current research, which has precluded detailed analysis of the relationship between *Chd4* heterozygosity, postnatal cortical development, and behaviour.

1.9 Hypothesis and Aims

We hypothesize that i) *Chd4* is required for neocortical (dorsal forebrain) neurogenesis and neurodevelopment and ii) that decrease or loss of *Chd4* expression leads to variations in behaviour.

1) We aim to generate and compare genetic mouse models of decreased or lost *Chd4* expression that more accurately recapitulate SIHIWES and that can be examined postnatally and to examine these mouse models for changes in forebrain development and/or cell composition.

2) We aim to assess our genetic mouse models of decreased or lost *Chd4* expression for meaningful variations in behaviour.

Chapter 2. Methods

2.1 Animal work

All animal work was approved by the University of Ottawa Animal Care Committee and carried out following guidelines set out by the Canadian Council of Animal Care. The University of Ottawa Animal Care and Veterinary Services facility provided animal housing, where animals were kept in a 12-hour light cycle with food and water provided *ad libitum*. All mouse lines were maintained on a C57BL/6J background. *CMV-Cre* mice were purchased directly from The Jackson Laboratory (B6.C-Tg(CMV-cre)1Cgn/J, Stock no. 006054). *Emx1-Cre+* mice were generously donated by Dr. David Picketts (OHRI, Ottawa, Canada). $Chd4^{f/f}$ founders were generously donated by Dr. Katia Georgopoulos (Harvard). *Emx1-Cre* mice and $Chd4^{f/f}$ mice were backcrossed to C57BL/6J background mice a minimum of six generations before experimentation began. Female $Chd4^{f/f}$ mice were crossed with male *Emx1-Cre+,* $Chd4^{f/+}$ mice to yield control (*Emx1-Cre-,* $Chd4^{f/+}$*; Emx1-Cre-,* $Chd4^{f/f}$) Chd4 conditional knockouts (*Emx1-Cre+,* $Chd4^{f/f}$) and conditional heterozygotes (*Emx1-Cre+,* $Chd4^{f/+}$). *CMV-Cre+* animals were crossed with $Chd4^{f/+}$ animals to yield control (C*MV-Cre-,* $Chd4^{+/+}$*; CMV-Cre-,* $Chd4^{f/+}$*; CMV-Cre+,* $Chd4^{+/+}$) and full body heterozygous (*CMV-Cre+,* $Chd4^{+/DEL}$) mice. All mice were included in our analyses with the exception of biological replicates where tissue was damaged, mice requiring euthanasia due to hydrocephalus (n = ~3), or when data was lost due to software malfunctions.

2.2 Genotyping

Ear clippings in adult mice or tail clippings in pre-natal/juvenile mice were collected. DNA was isolated with 50 mM NaOH at 95˚C for 20 mins followed by neutralization with 1M Tris pH 7.4,

vortex, and 5 min centrifuge spin (Legend Micro 21 Centrifuge, Sorvall, Thermo Scientific, Catalogue no. 75002437) at max speed. Polymerase chain reaction (PCR) was performed using primers listed in Table 1. Taq FroggaMix (Catalogue no. FBTAQM48, Frogga) was used for elongation and the thermocycler settings were as indicated in Table 2. Amplicons were run on 1.5% agarose gel (1.5% w/v agarose, 0.003% Ethidium Bromide in 1 X TAE Buffer (24.2% w/v Tris base, 5.7% glacial acetic acid, 50mM EDTA pH 8.0 in ddH2O), and visualizing using ultraviolet detection (Gel Doc XR+ Molecular Imager, Bio-Rad). Amplicon size was verified against 1kB DNA Ladder (GeneRuler 1 kb Plus DNA Ladder, Thermo Scientific, Catalogue no. FERSM1331). Mice used in behaviour studies were genotyped 2-3 times (one to two times before testing, once after testing) to confirm genetics. Mice denoted as "WT" include mice of the following genotypes: *Emx1-Cre-, Chd4*$^{+/+}$*; Emx1-Cre-, Chd4*$^{f/+}$*; Emx1-Cre-, Chd4*$^{f/f}$*; Emx1-Cre+, Chd4*$^{+/+}$*; CMV-Cre-, Chd4*$^{+/+}$*; CMV-Cre-, Chd4*$^{f/+}$*; CMV-Cre-, Chd4*$^{f/f}$*; CMV-Cre+, Chd4*$^{+/+}$.

Table 2. Polymerase Chain Reaction Thermocycler settings for *Chd4* Flox, *Chd4* DEL and *Cre* primers.

PCR Thermocycler Protocol	
Step 1	94˚C for 3:00 minutes
Step 2	94˚C for 0:30 minutes
Step 3	54˚C for 0:30 minutes
Step 4	72˚C for 1:00 minutes
Step 5	Repeat steps 2-4 35X
Step 6	72˚C for 10:00 minutes
Step 7	Hold at 12˚C

2.3 Dissection

Adult mice were euthanized via CO2 inhalation followed by cervical dislocation. The brains were dissected out, weighed, imaged, and fixed in 4% PFA overnight. Mouse pups were euthanized via decapitation, followed by brain dissection, imaging, fixing in 4% PFA overnight, and weighing. For immunohistochemistry, brains were subsequently transferred to 20% sucrose for 24 hours, freezing solution (1:1 of OCT:30% sucrose in PBS) for 24-36 hours, and frozen down to -80˚C in freezing solution.

2.4 Immunofluorescence

Brains were sectioned coronally using a Leica CM1860 cryostat. Thickness was set at 12μm for pre-natal brains and 16μm for post-natal brains. For consistency across coronal sections, the primary somatosensory cortex located between the crossing of the corpus collosum to the beginning of the hippocampus was targeted. Sections were rinsed in 1X PBS followed by antigen retrieval in citrate buffer (10 mM Sodium citrate, 0.05% Tween 20, pH 6.0) using a pressure cooker for 10mins, and rinsing with water for 10 minutes. All antibodies were diluted in 30% w/v Bovine Serum Albumin, 0.4% Triton, and 1:5000 Hoechst in PBS. Rat anti-Ctip2 (1:200, Abcam ab18465), Rabbit anti-Brn2 (1:200, Cell Signaling Technology 12137S), rat anti-Satb2 (1:100, Abcam ab51502), Rabbit anti-Tbr1 (1:100, Cell Signaling Technology 49661), Rabbit anti-Olig2 (1:200, Novus Biologicals NBP1-28667SS), rabbit anti-Aldh1l1 (1:100, Abcam ab87117), mouse anti-Chd4 (1:200, Abcam ab70469), rat anti-Chd4 (BioLegend 942302, 1:100), rabbit anti-Chd4 (Abcam ab72418, 1:100), goat anti-Sox2 (R&D Systems AF2018, 1:200), rabbit anti-Neurog2 (Cell Signaling Technology 13144S, 1:250), mouse anti-Pax6 (Developmental Studies Hybridoma Bank PAX6, 1:10), and rabbit anti-Tbr2 (Abcam ab23345,

1:100) primary antibodies were left overnight at 4˚C, followed by three 1X PBS washes, secondaries (Alexa Fluor 488 goat anti-mouse IgG (Jackson ImmunoResearch 115-545-003; 1:1000), DyLight 550 donkey anti-rat IgG (Invitrogen SA510027; 1:1000), Dylight 650 donkey anti-rabbit IgG (Novus Biologicals NBP1-75634; 1:1000)) were incubated for 1 hour at room temperature, three 1X PBS washes and mounted in Mowiol mounting media (12% w/v Mowiol 4-88, 30% w/v glycerol, 120mM Tris-Cl pH 8.5, 2.5% DABCO).

2.5 Cell Counting and imaging

Every other section, barring imperfections, was imaged using the Zeiss LSM900 Confocal Microscope at 200X magnification. Single Z-stack images were tiled and stitched using Zeiss software. Manual cell counting was performed using Adobe Photoshop on 200µm-wide sections of somatosensory cortex between the crossing of the corpus callosum and the start of the hippocampus. Each 200µm-wide section was separated into six 200µm-wide bins of equal height for counting. This allowed the proportion of cells in the upper sixth area of the cortex to the lower sixth area of the cortex to be assessed, as well as total (i.e. absolute) counts. Three technical replicates were counted for each biological replicate.

2.6 Cortex area and cerebellum area measurements

Brains were imaged post-dissection using the Zeiss Stemi 508 stereo microscope with Axiocam ERc 5s at 6.3X magnification. Images were imported into Fiji and the outline of cortex or cerebellum was traced using the "polygon selections" tool. Area measurements were recorded and used for subsequent analysis. Scale was consistent across images and is depicted with arbitrary units.

2.7 Statistics

Data is presented as mean ± standard deviation unless otherwise indicated. Round black circles represent individual data points. Emx1-Cre vs CMV-Cre lines were assessed separately due to significant differences between the control groups of both lines (see Figure 3.3C, E; Figure 3.4D; Figure 3.5 C, D, E and control lanes in Figure 4.9 B/E, D/G; Figure 4.11B/G, C/H, D/I; Figure 4.12B/D for examples). Statistical analysis of two groups or three groups was performed vs Student's t-test, or one-way ANOVA with Tukey's post-hoc tests (as indicated in the figure legends/text), respectively. $P < 0.05$ was considered statistically significant. All statistical analyses and graphs were performed/generated using GraphPad Prism version 8.0.0 for OS X, GraphPad Software, San Diego, California USA, www.graphpad.com.

2.8 Behaviour analysis

Behaviour testing, including protocols and materials provided, was done with the Behavioural Core Facility at the University of Ottawa. Mice were assessed between ~3-8 months of age, with females and males housed separately. Mice were habituated to testing room for at least 30 minutes prior to commencing testing. Mice were handled (lifted out of cage and put back 3-4 times) for 5 days prior to testing commencing. Testing was scheduled so that mice only performed one behaviour test a day following established protocols. Behaviour testing was recorded with a video camera mounted appropriately and subsequently analyzed using Ethovision software (Noldus). Velocity and distanced travelled measurements were captured during each behaviour test. During analysis, male and female data was pooled, as no sex-specific significant differences were observed, unless otherwise indicated. One female gHT mouse died during behaviour testing, hence some of the tests only have biological replicates of five female

gHT instead of six. Additionally, one batch of mice was not subjected to the elevated plus maze during testing, explaining why the biological replicates are lower in this test compared to others. All testing was performed blind to animal genotype.

Elevated Plus Maze

Mice were placed in the middle of a plus shaped apparatus that was elevated above the ground for 10 minutes under 100 lux lighting. Two arms of the plus maze, opposite to each other, were enclosed (6 cm wide x ~69cm long, 20 cm high walls) while the remaining two were open (6 cm wide x ~69cm long, raised 74 cm off the floor). The number of entries the mouse made into the closed versus open arms, as well as the time spent in the closed versus open arms was measured. Measurements of mice activity, videos of mice activity, and analysis was collected using Ethovision software (Noldus).

Open Field

Mice were placed in the middle of an opaque plastic box (45 cm x 45 cm x 45 cm) with an open top. A camera mounted above the box recorded the mice activity for 10 minutes under 300 lux light. Ethovision software (Noldus) was used to analyze videos of mice activity. The amount of time mice spent in the center of the box (small centre and large centre) and the corners of the box was recorded. The latency for the mice to reach the corners of the box was also measured.

Beam Break

Mice were placed in a new housing cage that was placed between a photocell emitters and photocell receptors system for 24 hours. Disruption of the infrared light as the mouse

moved through the cage was detected and recorded by the photocell analyzer (Micromax Analyzer, AccuScan) and subsequently tallied through computer analysis (Fusion 5.3 software, Omnitech Electronics Inc.). Ambulatory Activity Counts, measuring the amount of beam breaks that occurred while the animal was ambulating (vs stereotypic behaviour such as grooming, etc.) was plotted. Unfortunately due to a software malfunction, data was lost during the first three to four hours of testing for one cohort of mice, which included 13 WTs, 3 *Chd4* cHTs and 4 *Chd4* cKOs. This can explain the jump in data of the cKOs between 12:30-13:30 (See Figure 4.7).

Marble Burying

Mice were first habituated to the testing arena with no marbles present for 5 minutes. Subsequently, 20 marbles were evenly spaced atop woodchip bedding in a 4 x 5 marble grid in the arena. Mice were placed in the testing area again for 30 minutes and the number of marbles buried after this time was manually recorded. 75%+ of marbles covered by bedding was considered as buried.

Adult Social Interaction

Mice were habituated in red light before testing, and the test was subsequently performed under red light. During the habituation phase, a mouse was placed in the corner of a 45 cm x 45 cm x 45 cm box with a 5.5 cm x 9.6 cm wire mesh rectangular cage located along one side and allowed to explore for 5 minutes. After this point, the mouse was removed and temporarily placed in a clean container for 5 minutes. Next, a C57BL/6J background social target mouse (of the same gender and of similar age) was placed inside

the wire mesh cage for the socialization phase. The tested mouse was reintroduced into the box for 5 minutes and activity recorded. Time spent and number of entries of the mouse's body near the cage (large interaction zone) and in the corners was recorded, as well as time and number of entries the nose point of the mouse entered the small interaction zone around the cage.

Rotarod

Mice were placed on a horizontal textured rod (IITC Life Science, Ugo Basile) rotating at a speed of 5 RPM. The speed was gradually increased to 40 RPM over the course of five minutes and the time the mouse spent on the rod before falling off (latency to fall) was recorded. Mice were trained on the Rotarod four times a day with 10 minute intertrial intervals in their home cage. This was performed for four consecutive days.

Morris Water Maze

A ~132cm diameter pooled was filled with opaque (white non-toxic tempura paint) water (22˚C) with a 10cm diameter white platform hidden 1cm below the surface of the water. The pool had 4 starting location at the edge of the pool located equidistant to each other, and the platform was located between two of them about 24cm from the edge of the pool. Lighting was set to 140 lux and the pool was surrounded by 4 white "walls". Two black visual cues were located on two of the adjacent walls to allow for spatial navigation. Briefly, a mouse was placed in the water at one of the starting points and allowed to try and find the platform for 1 minute. If they did not find it, the platform was tapped by the researcher, and if the mice still did not find it, gently guided by the tail towards the

platform. Once on the platform, the mouse was left for 10 seconds, prior to being removed, toweled off and returned to its home cage for a 15-minute intertrial interval. Mice were trained 4 times a day at each of the locations, the order of which was randomized. After 6 days of training, the platform was removed and the amount of time the mouse spent in the quadrant where the platform was located, and the number of times the mouse crossed the area where the platform had been was measured.

2.9 Optomotor Analysis

The StriaTech Optodrum was used to assess visual acuity in mice. Briefly, a mouse was placed atop a white 9 cm diameter platform in the middle of the OptoDrum (box shaped). Contrast cycles were set at 99.72% with a constant rotation speed of 12˚/s. The number of cycles was set to start at 60 cycles (0.167 cyc/˚) and increased/decreased following an automatic staircase procedure that allowed determination of visual acuity (i.e., max number of cycles mice would respond to). Mice were tested for three consecutive trials in one day and the mean of these trials was calculated and graphed.

Chapter 3. Characterizing cortical growth in *Chd4* mouse models

3.1 Characterizing *Chd4* expression and generation of *Chd4* mouse models

It is generally thought that *Chd4* is ubiquitously expressed throughout cell types and tissues. To examine Chd4 expression during neocortical development, we performed a comprehensive set of co-stainings with cell type-specific marker proteins (Figure 3.1). We found that Chd4 appeared fairly ubiquitously expressed, with co-expression in neural progenitor cells (Pax6), intermediate progenitor cells (Tbr2), early born/deep layer neurons (Tbr1, Ctip2), late born/upper layer neurons (Brn2, Satb2), and a subset of glia cells (Olig2, Aldh111) among others. Hence, we generated a detailed reconstruction of *Chd4* expression during cortical development and found that Chd4 is present and may play a role in various cell types.

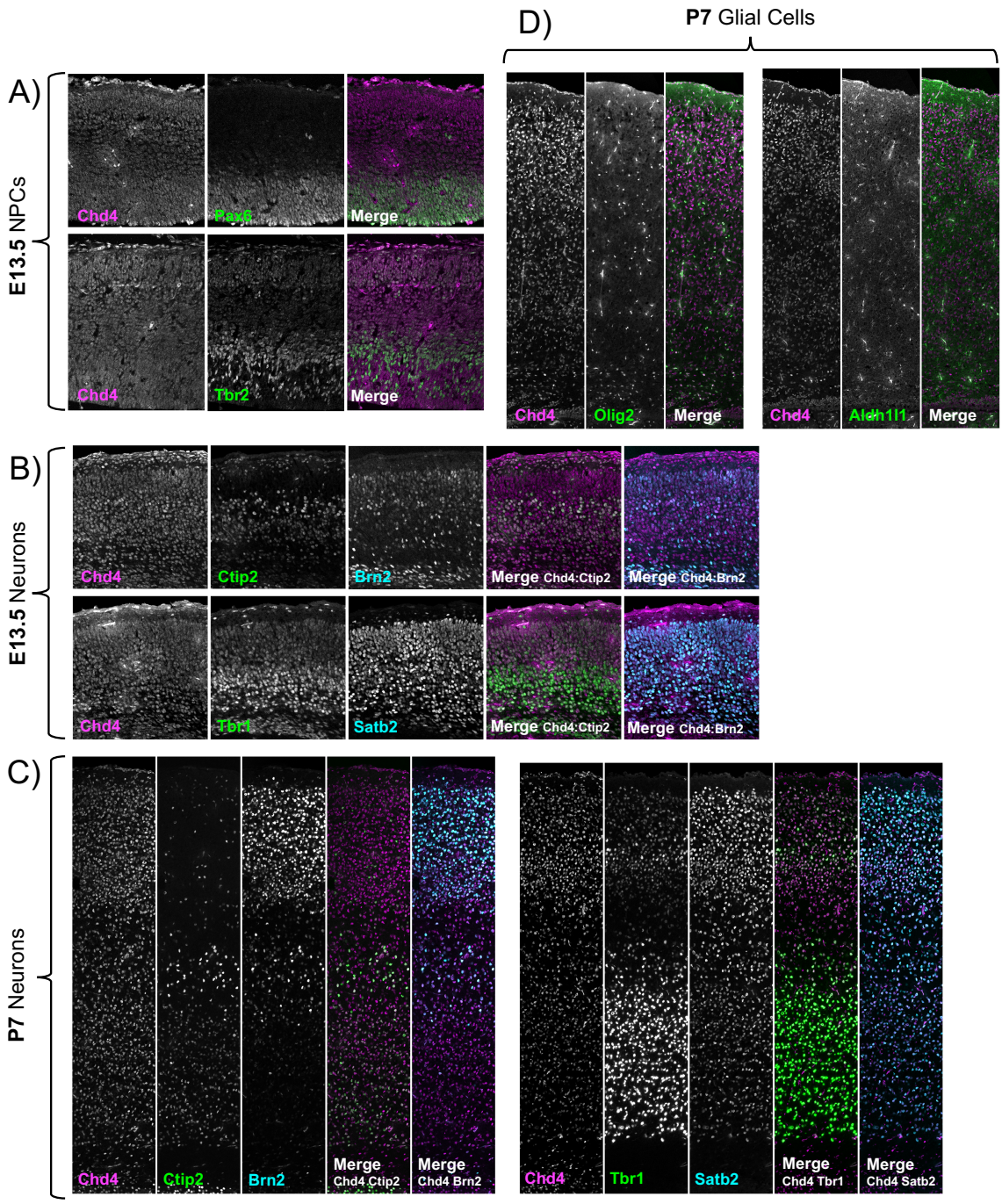

Figure 3.1. *Chd4* is expressed in various neural cell types throughout development. A-D) Co-staining of Chd4 with NPC markers Pax9 and Tbr2 (A), upper layer neuron markers Brn2 and Satb2 (B, C), deep layer neuron markers Ctip2 and Tbr1 (B, C) and glial cells markers Olig2 and Aldh1l1 (D) at E13.5 and/or P7 stages in murine cortex. Chd4 co-staining with neuron markers also observed at E14.4, E17.5, P0, and P30 stages (not shown).

In order to assess the role of *Chd4* in neurodevelopment and behaviour, we generated and characterized mouse lines with reduced or conditionally ablated *Chd4* expression. We took advantage of a previously developed mouse line that allows for conditional knockout of the *Chd4* ATPase domain (exons 12-21) using a Cre/loxp approach[113], as most identified individuals with Sifrim-Hitz-Weiss syndrome present with missense mutations in the SNF2-like domains of *Chd4* (Figure 3.2A). Previous work suggests that loss of these exons will inactivate *Chd4* and lead to reduced full length mRNA and protein levels, allowing for a *Chd4* knockout phenotype[113]. To validate this, we used an antibody targeting an epitope outside of the ATPase domain in our *Chd4* conditional knockouts and found that Chd4 staining was greatly reduced in the somatosensory cortex (Figure 3.2B). We believe the remaining Chd4 expression in the cortex was due to cells that fell outside of our Cre-driver (*Emx1-Cre*) lineage, including inhibitory cortical neurons.

All individuals with SIHIWES identified to date are heterozygous. Hence, we crossed mice heterozygous for the *Chd4* floxed exons with *CMV-Cre*, a ubiquitous-Cre driver to examine full body (germline) heterozygous $Chd4^{+/DEL}$ mice (*Chd4* gHTs), which we predicted would better model the human genetics. We additionally sought to more deeply investigate *Chd4*'s role in the cortex, as SIHIWES presents very frequently with intellectual disability, suggesting a role for *Chd4* in the executive and associative centers of the brain. Moreover, patients frequently exhibit macrocephaly, and Nitarska et al. previously found cortical growth phenotypes[84]. However, the *Nestin-Cre* driver used by Nitarska et al. is expressed throughout the neural tube at very early stages (~E7.75[114]), and led to perinatal lethality[84]. To ablate *Chd4* in a later (~E9.5) and more restricted fashion, we used an *Emx1-Cre* driver[115] to target the dorsal telencephalon, which gives

rise to the cortex, in order to generate *Chd4* conditional knockouts (*Chd4* cKOs) and conditional heterozygotes (*Chd4* cHTs) (Figure 3.2A). The *Emx1-Cre* driver was found to be largely specific to the cortex (Figure 3.2C), although we did observe some Cre expression in the hypothalamus, hippocampus and in the dermis (not shown, however confirmed in the literature)[115]. As previous work indicates germline homozygous mice will be lethal, we excluded them from our study[84,108]. We found that all mouse models were viable. However, we observed significantly less *Emx1-Cre+; Chd4*$^{flox/flox}$ mice than expected following Mendelian ratios (Table 3). A few mice in the *Emx1-Cre* line also presented with hydrocephalus requiring euthanasia around P30, with one confirmed to be a *Chd4* cKO (Figure 3.2D). Additionally, a small subset of adult *Chd4* cKOs presented with what appeared to be benign skin growths/lesions, possibly as a result of the *Emx1-Cre* driver expressing in the dermis (data not shown), where it was previously shown to be required for barrier function[116]. Brief examination of the hippocampus in *Chd4* cKOs also revealed apparent defects in development relative to wildtype, with the dentate gyrus appearing almost completely abolished (Figure 3.2E). *Chd4* cHTs and gHTs were generated in expected Mendelian numbers (Table 3 and Table 4, respectively), though there were more WT mice than expected generated in our *Chd4* gHT crosses. The Cre allele is also thought to be x-linked in this model, which may help explain the slight change in numbers.

Chd4 cKOs, cHTs and gHTs were identified by PCR genotyping and validated by immunohistochemistry (Figure 3.2 B, F, G). Western Blot analysis (not shown) revealed that Chd4 was still expressed in *Chd4* gHTs.

Table 3. Mendelian Ratios of *Chd4* cHT and cKO mice. *Emx1-Cre+; Chd4*$^{Flox/+}$ mice were crossed with *Chd4*$^{Flox/Flox}$ mice to yield *Chd4* conditional heterozygotes and conditional knockouts. Data was retrieved from two P7 litters (2 *Chd4* cKO / 17 mice) and litters post weaning. Probability based off Chi-square vale was calculated. Degrees of Freedom = 3.

***Emx1-Cre+; Chd4*$^{f/+}$ x *Chd4*$^{f/f}$**	***Chd4*$^{f/f}$**		***Chd4*$^{+/f}$**	
	Emx1-Cre-	***Emx1-Cre+***	***Emx1-Cre-***	***Emx1-Cre+***
Expected	19.25	19.25	19.25	19.25
Observed	34	3	14	26
Chi-square value	11.30195	13.71753	1.431818	2.366883
Probability	0.05*	0.01**	n.s.	n.s.

Table 4. Mendelian ratios of *Chd4* gHT. *CMV-Cre+; Chd4*$^{+/DEL}$ mice were crossed with *CMV-Cre+* mice to yield *Chd4* germline heterozygotes. Data was retrieved from four P7 litters (5 *Chd4* gHT / 22 mice) and litters post weaning. Probability based off Chi-square vale was calculated. Degrees of Freedom = 3.

***CMV-Cre+ x CMV-Cre+ Chd4*$^{+/DEL}$**	***Chd4*$^{+/+}$**		***Chd4*$^{+/DEL}$**	
	Cre-	***Cre+***	***Cre-***	***Cre+***
Expected	9.625	28.875	10.75	28.875
Observed	29	22	7	19
Chi-square value	39.00162	1.97153	1.30814	3.82243
Probability	0.01*	n.s.	n.s.	n.s.

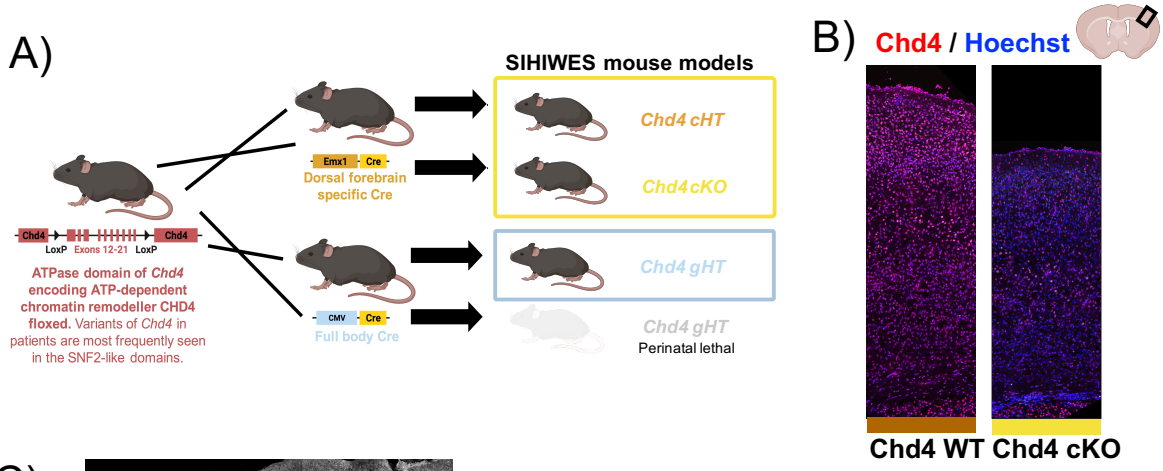

C)

Emx1-Cre+ expression

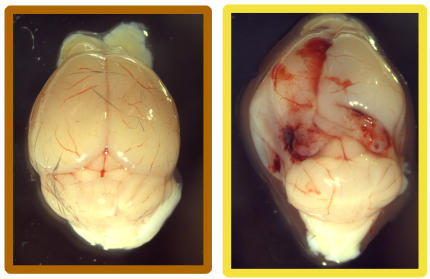

D)

Chd4 WT

Chd4 cKO with hydrocephalus

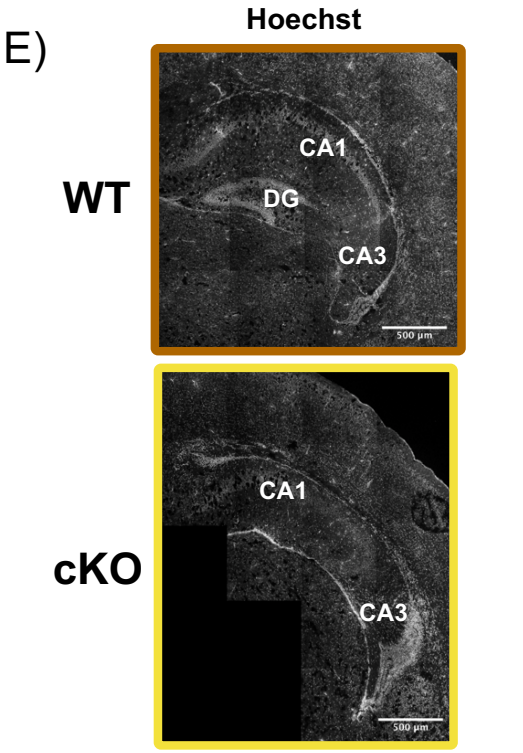

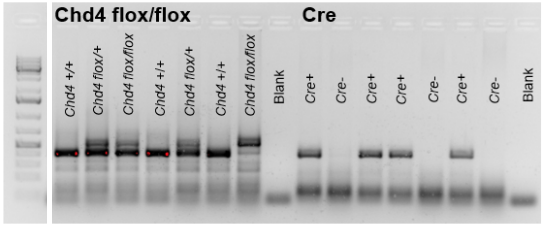

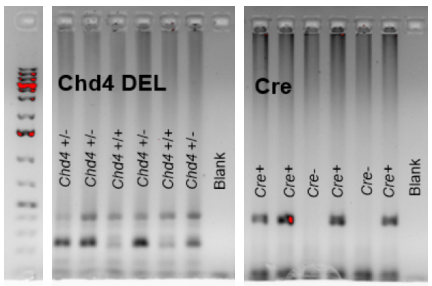

Figure 3.2. Creating three *Chd4* mouse models to understand SIHIWES. A) Mouse model strategy. A mouse with a floxed ATPase domain of *Chd4* was crossed with an *Emx1-Cre* driver to yield conditional heterozygotes (cHTs) and conditional knockouts (cKOs) specific to the dorsal telencephalon. The floxed ATPase mouse was also crossed to *CMV-Cre+* mice to yield germline heterozygotes (gHTs). Created with BioRender.com. **B)** Staining of P7 brain in a wildtype and Emx1-Cre *Chd4* conditional knockout demonstrating loss of Chd4 staining in the brain. The antibody used mapped outside of the floxed ATPase domain of Chd4, suggesting loss of Chd4 protein. **C)** Staining of YFP in *Emx1-Cre+, ROSA-YFR/YFP* P2 mouse brain, showing pattern of *Emx1* expression in the cortex. **D)** Example of Chd4 cKO mouse brain with hydrocephalus compared to wildtype. **E)** Coronal sections of hippocampus with Hoechst staining in WT (top) and cKO (bottom) brains. **F)** Example of genotyping for WT, cHT, and cKO mice with Chd4 and Cre PCR primer sets. **G)** Example of genotyping for the DEL locus (i.e. locus after floxed ATPase domain is spliced out) and generic Cre.

3.2 Characterizing gross anatomy of *Chd4* mouse models

We sought to examine our mouse models for changes in the gross anatomy and cell composition of the brain (see Table 5 for summary of findings). Due to differences observed between the *CMV-Cre* and *Emx1-Cre* control animals (see Figure 3.3C, E; Figure 3.4D; Figure 3.5 C, D, E as examples), we chose to analyze *Chd4* cHTs and cKOs separately from gHTs. P7 mice were examined for changes in body weight, brain weight, and area of the cortex (arbitrary units, measured from images looking down on the dissected brain). *Chd4* cKOs presented with significant decreases in brain weight and cortex area (Figure 3.3A-C). However, the size of the cerebellum remained unchanged (Figure 3.3D). This suggests that the decrease in brain weight was largely driven by the loss of cortex mass. This is in accordance with the predicted expression pattern of *Emx1-Cre* within the telencephalon but not the cerebellum, and also matches well with previous findings of decreased brain weight in E18.5 *Nestin-Cre Chd4* cKOs[84].

Chd4 gHTs also presented with decreased brain weight (Figure 3.3B) and cortex area (Figure 3.3C), but not cerebellum area (Figure 3.3D) or overall mass (Figure 3.3E), which suggests that the loss in brain mass may also be due to decreased cortical tissue. Interestingly, however, the change in cortex area was a lot less than that observed in *Chd4* cKO, despite a similar decrease in brain weight of both models. This might suggest that the loss of brain mass in *Chd4* gHTs is additionally due to subcortical structures. Meanwhile, *Chd4* cHTs appeared to exhibit no overt changes of gross anatomy relative to wildtype (Figure 3.3). This suggests that Chd4 likely has important roles in very early in cortical development prior to the expression of *Emx1-Cre*, supporting existing literature[84,108].

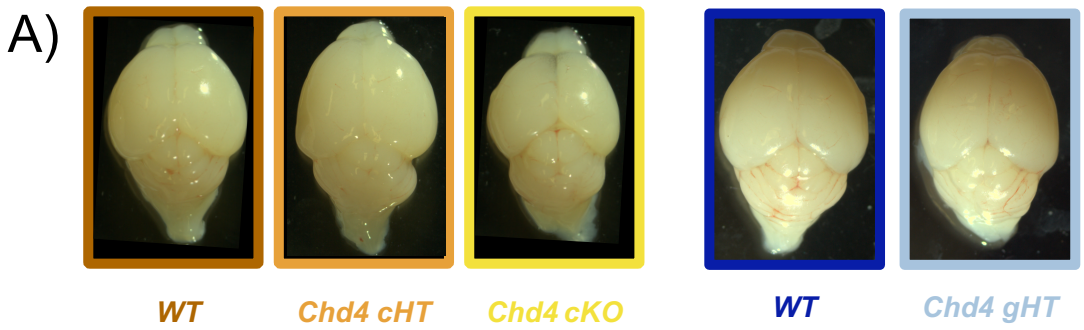
A)
WT
Chd4 cHT
Chd4 cKO
WT
Chd4 gHT

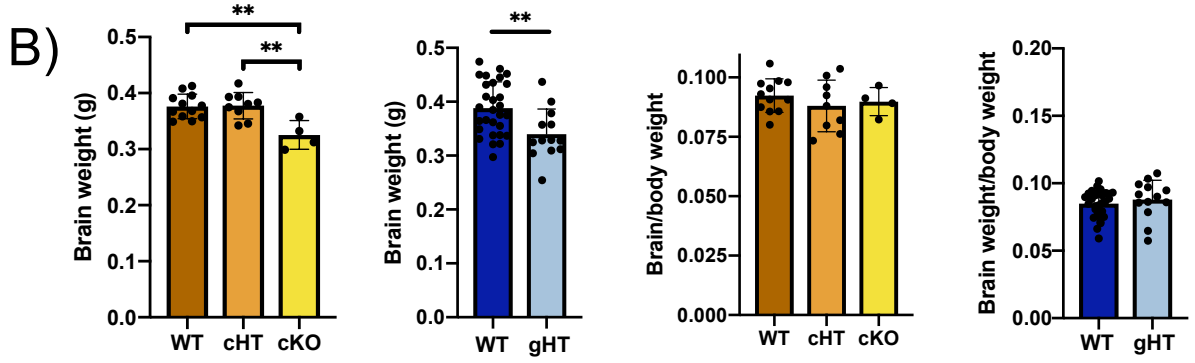
B)
Brain weight (g)
WT cHT cKO
Brain weight (g)
WT gHT
Brain/body weight
WT cHT cKO
Brain weight/body weight
WT gHT

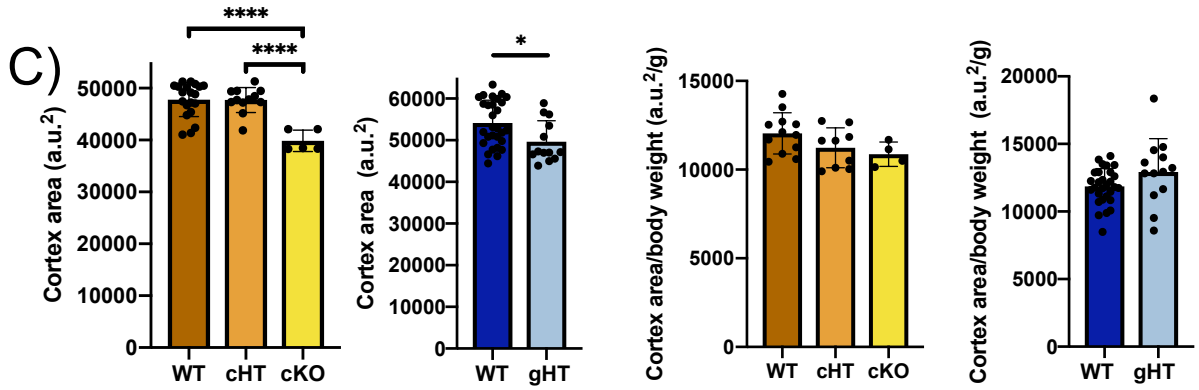
C)
Cortex area (a.u.2)
WT cHT cKO
Cortex area (a.u.2)
WT gHT
Cortex area/body weight (a.u.2/g)
WT cHT cKO
Cortex area/body weight (a.u.2/g)
WT gHT

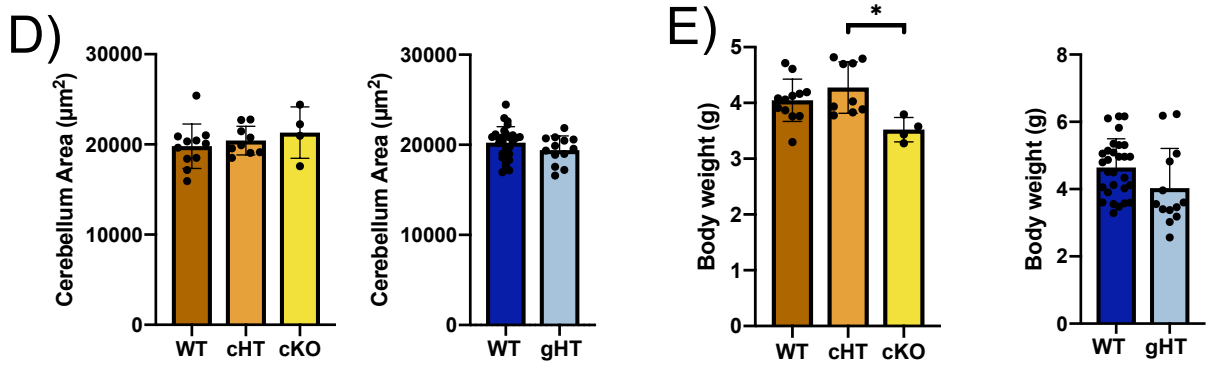
D)
Cerebellum Area (µm2)
WT cHT cKO
Cerebellum Area (µm2)
WT gHT
E)
Body weight (g)
WT cHT cKO
Body weight (g)
WT gHT

Figure 3.3. *Chd4* is required for cortical growth. A) Images of P7 WT, *Chd4* cHT and *Chd4* cKO brains (*Emx1-Cre* line, left) and WT and *Chd4* gHT brains (*CMV-Cre* line, right). **B)** Brain weight (left) and brain weight/body weight (right) of *Chd4* cHT, cKO, and gHT mouse models and respective controls. **C)** The cortex was traced using images of the brain (as in A) and area was calculated. Cortex area of all *Chd4* mouse models relative to respective controls (right), and of cortex area/body weight (left) are shown. **D)** Area of the cerebellum was traced as described above and calculated for WT, cHT and cKO mice (right). The proportion of cortex area relative to cerebellum area was also calculated (left). **E)** Body weight of WT, cHT, cKO and gHT mouse models. All statistical analyses are via One-way ANOVA with Tukey's post-hoc test (*Emx1-Cre line*) or unpaired Student's t-test (*CMV-Cre line*). * $p < 0.05$. ** $p < 0.01$. **** $p < 0.0001$. Biological n = 12 (WT-*Emx1*), 6 (cHT), 4 (cKO), 29 (WT-*CMV*), and 13 (gHT), with the exception of D) wherein n = 28 (WT-*CMV*), as one cerebellum was damaged during dissection.

To further investigate changes in cell numbers and composition within the cortex, we generated coronal sections of the somatosensory cortex between the crossing of the corpus callosum to the beginning of the hippocampus. We proceeded to measure the thickness of the somatosensory cortex, thickness of white matter under the cortex, total cell number in the cortex (via Hoechst staining) and cell density. At the histological level, the decreased cortex area in *Chd4* cKOs corresponded to decreased cortex thickness (Figure 3.4A, B), decreased thickness of white matter (Figure 3.4C) and decreased number of Hoechst+ cells (Figure 3.4D), though overall cell density remained unchanged (Figure 3.4E). *Chd4* cHTs were largely similar to wild-type mice, however, they presented with a small but significant increase in thickness of the white matter layer under the cortex (Figure 3.4C). The observed decrease in cortical area in *Chd4* gHTs did not affect the thickness of the cortex in cross-section, though there was a non-significant trend of the *Chd4* gHTs having decreased cell number (Figure 3.4D) and cell density (Figure 4E). *Chd4* gHT had significantly decreased cell number in a subset of bin counts, supporting the decreased cell number trend (Figure 3.4 D).

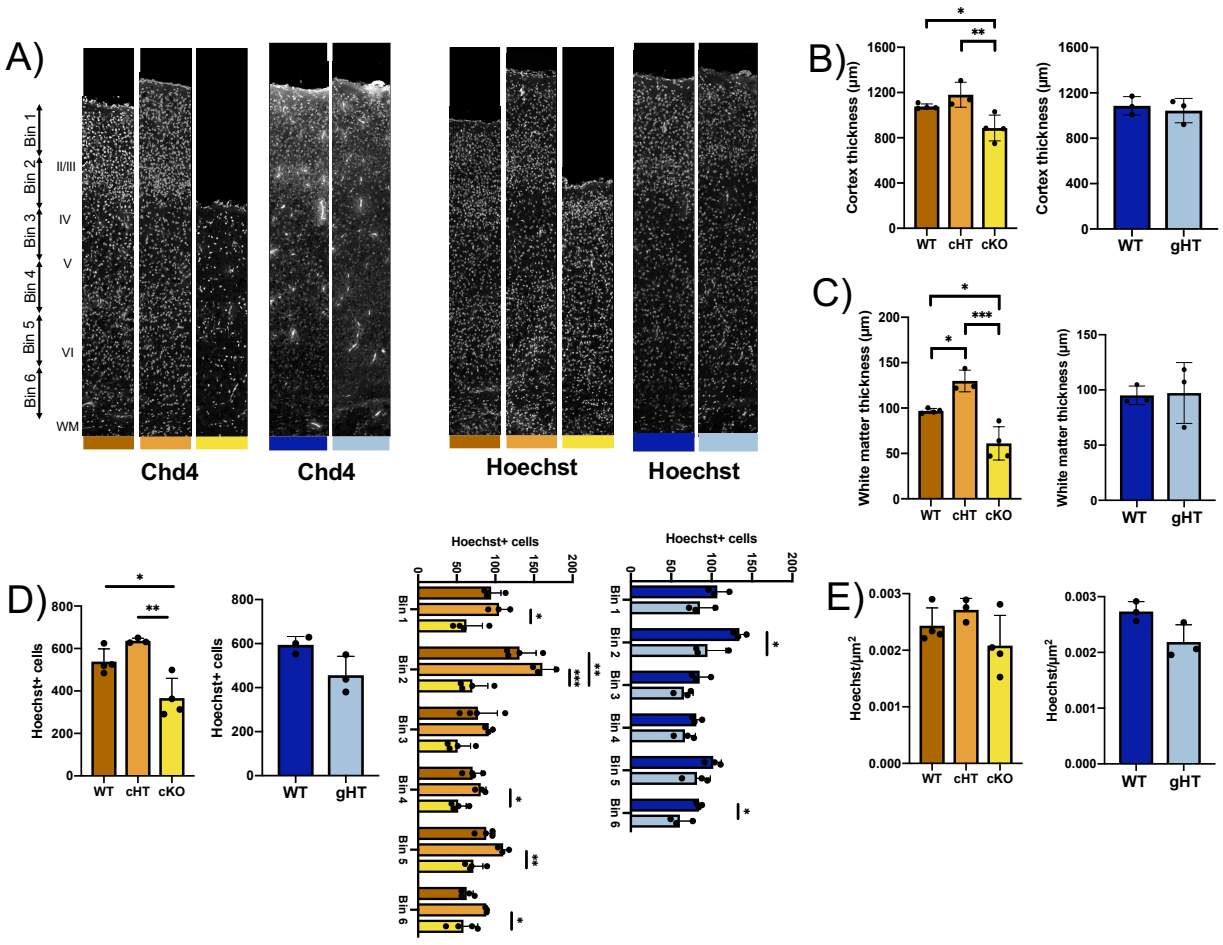

Figure 3.4. Changes in cortex thickness and cell number in *Chd4* mouse models. A) Sample images of Chd4 and Hoechst immunohistochemistry in *Chd4* cHT, cKO, and gHT mouse models and respective controls in coronal sections of the P7 somatosensory cortex. **B)** Cortex thickness and **C)** thickness of white matter layer below cortex in *Chd4* cHT, cKO, and gHT mouse models and respective controls. **D)** Total number of Hoechst positive cells (left) and number of Hoechst+ cells per bin (right) in *Chd4* cHT, cKO, and gHT mouse models and respective controls. Bins are 200µm in width (tangential axis) and equally sized per sample (adjusted to cover the radial axis) in height. **E)** Cell density of somatosensory cortex in *Chd4* cHT, cKO, and gHT. All statistical analyses are via One-way ANOVA with Tukey's post-hoc test (*Emx1-Cre line*) or unpaired Student's t-test (*CMV-Cre line*). * $p < 0.05$. ** $p < 0.01$. *** $p < 0.001$. Biological n = 4 (WT-*Emx1*), 3 (cHT), 4 (cKO), 3 (WT-*CMV*), and 3 (gHT).

3.3 Characterizing cell composition of *Chd4* mouse models

To better understand the changes in cortex area in our *Chd4* mouse models, we performed immunohistochemistry on the P7 somatosensory cortex sections using markers for neuronal (Figure 3.5) and glial (Figure 3.6) cells. This included late-born upper layer markers (*Brn2, Satb2*), early-born deep layer markers (*Ctip2, Tbr1*), and glial markers (*Olig2, Aldh1l1*). We analyzed these counts in terms of the absolute number of cells (Figure 3.5 and Figure 3.6) or the proportion of cell subtypes over total Hoechst (Supplementary Figure 1). Additionally, we divided the coronal somatosensory cortex into 6 equally sized bins per section, allowing for cell distribution across the cortex in the radial axis (top to bottom) to be assessed.

Chd4 cKOs presented with a decrease in late-born upper layer Brn2+ cells and Satb2+ cells (Figure 3.5A, B, C). Lower layer neural (Figure 3.5A, D, E) and glial (Figure 3.6A, B, C) cell markers remained unchanged. This is also consistent with previous findings, wherein *Nestin-Cre Chd4* cKOs present with decreased production of upper layer markers due to impaired proliferation of neural progenitor cells[84]. Conversely, we also observed an increase in the number of Ctip2+ Brn2+ double positive cells in our *Chd4* cKOs, which are largely located in the deep layers (Figure 3.5F-H). Potentially, this may represent mixed neuron identities or an expansion of a rare subtype of Ctip2 Brn2 double positive cells. Together, this suggests that our *Chd4* cKO have decreased upper layers leading to decreased cortex size, and potentially some minor changes in cell identity or neural subtypes.

Chd4 cHTs presented with no changes in neural markers (Figure 3.5) or overall numbers of glial cells (Figure 3.6). However, bin distribution of cells revealed that *Chd4* cHTs presented with a

slight increase in Olig2+ cells in the upper area of the cortex (Figure 3.6B). This is interesting due to the change in white matter previously noted below the cortex (Figure 3.4C) and suggests that *Chd4* cHTs may have altered white matter.

Though *Chd4* gHTs presented with a trend towards decreased late-born upper layer Brn2+ cells, the number did not come to significance (Figure 3.5B). Instead, we found that *Chd4* gHTs had a slight decrease of early-born deep layer *Ctip2*+ cells (Figure 3.5D). As this decrease in *Ctip2*+ cells did not affect cortex thickness (Figure 3.4B), but trended towards decreased overall cell number (Figure 3.4D, E), it suggests that the *Chd4* gHTs present with a specific decrease in *Ctip2*+ positive cells. Potentially, this reduction in cells may have also contributed towards the observed decrease in cortex area (Figure 3.3C), which might indicate decreased cortical growth in the tangential axis more than along the radial axis. Alternatively, the decrease in Ctip2+ cells appears most striking in bins 1, 2 and 5 (Figure 3.3C), which are outside of the area where layer 5 Ctip2+ cells reside. This might suggest that the loss of Ctip2+ cells indicates a more restricted expression of Ctip2 in cells versus a loss in cells overall.

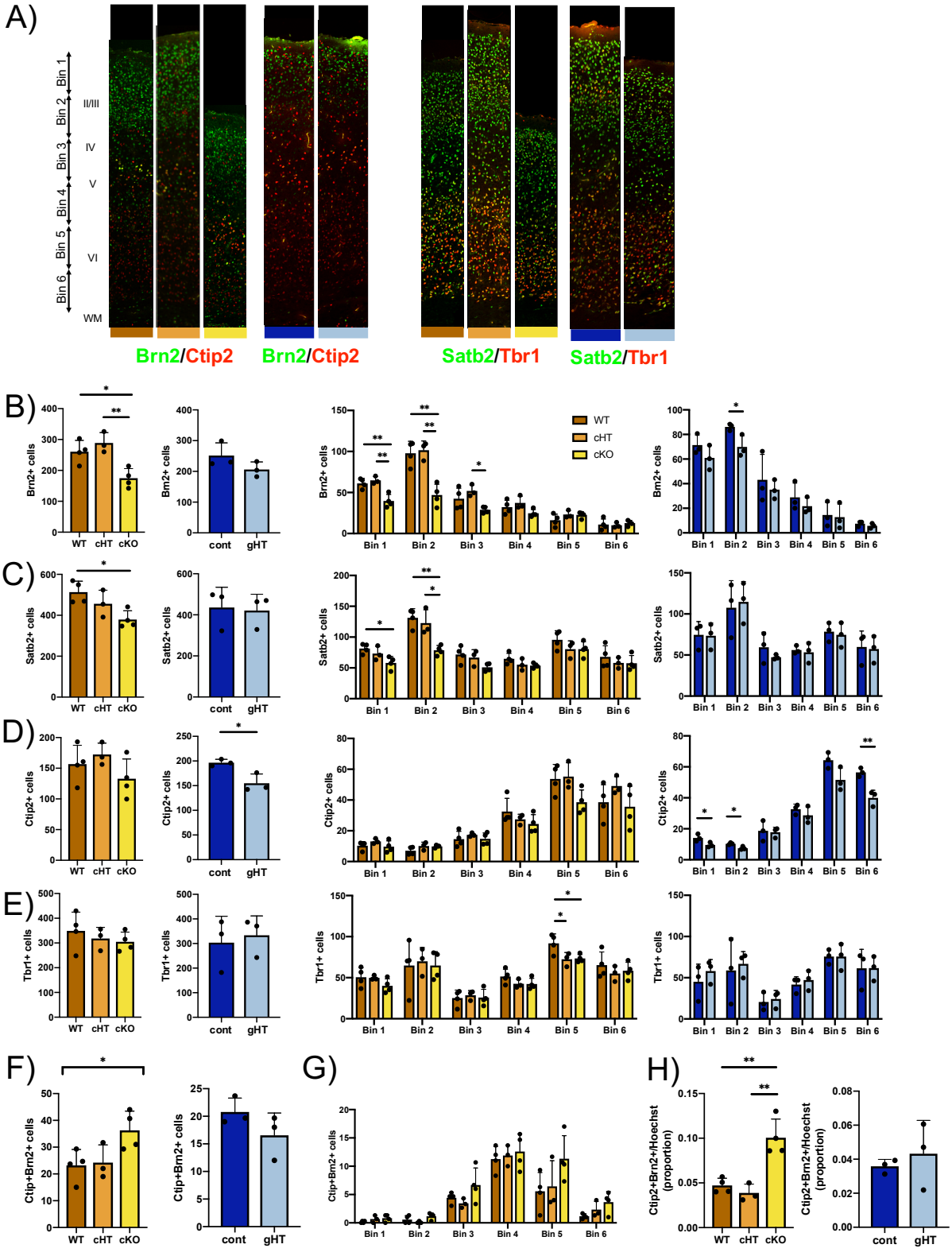
A)
Bin 1
Bin 2
Bin 3
Bin 4
Bin 5
Bin 6
II/III
IV
V
VI
WM
Brn2/Ctip2
Brn2/Ctip2
Satb2/Tbr1
Satb2/Tbr1
B)
Brn2+ cells
WT
cHT
cKO
cont
gHT
Bin 1
Bin 2
Bin 3
Bin 4
Bin 5
Bin 6
C)
Satb2+ cells
D)
Ctip2+ cells
E)
Tbr1+ cells
F)
Ctip+Brn2+ cells
G)
Ctip+Brn2+ cells
H)
Ctip2+Brn2+/Hoechst (proportion)

Figure 3.5. *Chd4* is required to expand upper layer neocortical neurons. A) Sample images from P7 coronal sections of the somatosensory cortex for layer-specific marker proteins as indicated. **B-G)** Total absolute cell counts and absolute cell counts per bin of neuron markers Brn2 (B), Satb2 (C), Ctip2 (D), Tbr1 (E), and Brn2 Ctip2 double positive cells (F, G) in *Chd4* cHT, cKO, and gHT mouse models and respective controls. **H)** Proportion of Brn2 Ctip2 double positive cells over Hoechst in *Chd4* cHT, cKO, and gHT mouse models. All statistical analyses are via One-way ANOVA with Tukey's post-hoc test (*Emx1-Cre line*) or unpaired Student's t-test (*CMV-Cre line*). * $p < 0.05$. ** $p < 0.01$. Biological n = 4 (WT-*Emx1*), 3 (cHT), 4 (cKO), 3 (WT-*CMV*), and 3 (gHT).

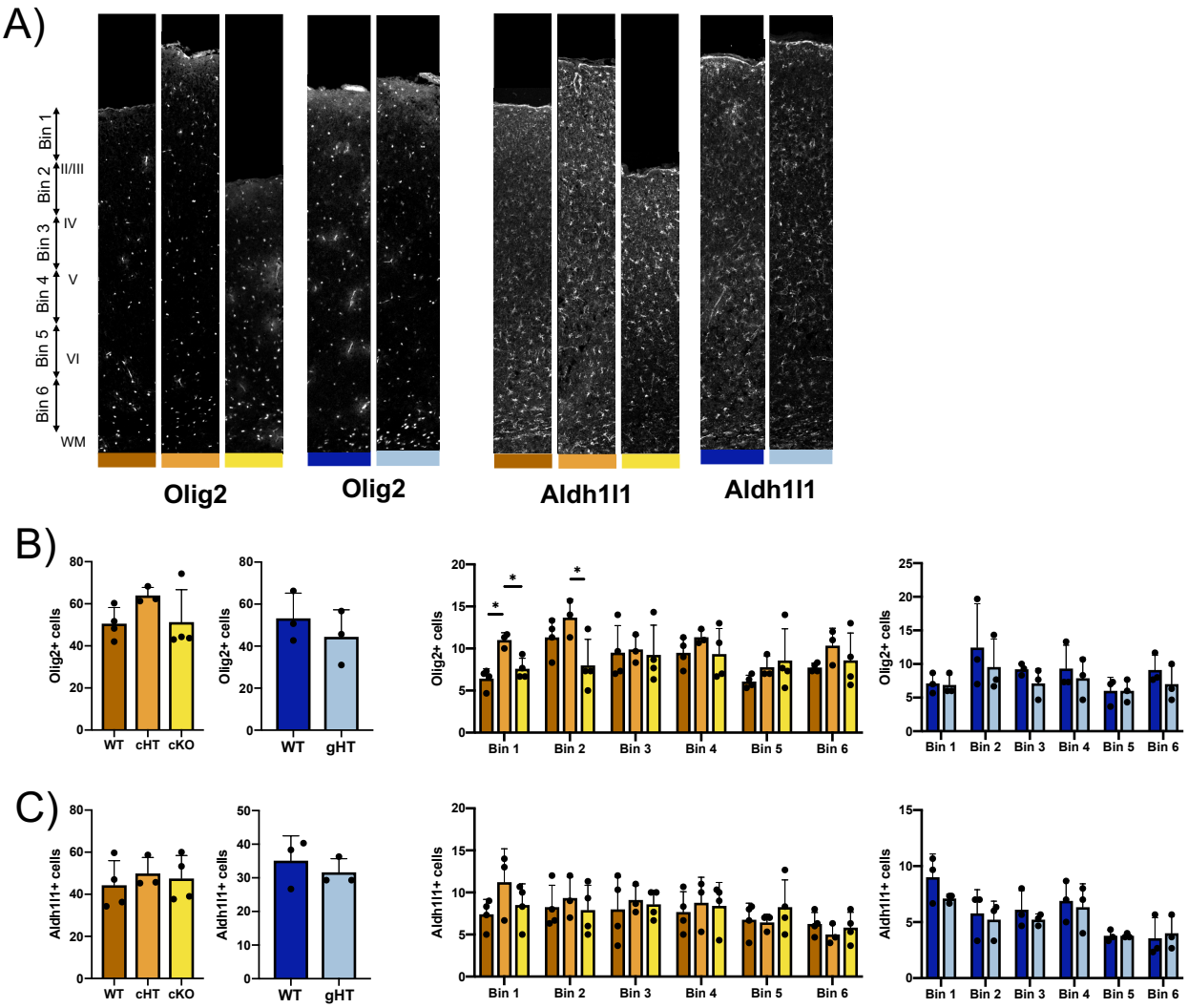

Figure 3.6. Investigating glia composition in P7 *Chd4* cHT, cKO and gHT mouse models. A) Sample images from P7 coronal sections of the somatosensory cortex for glial-specific marker proteins as indicated. **B-C)** Absolute cell counts and absolute cell counts per bin of glial markers Olig2 **(B)** and Aldh1l1 **(C)** in *Chd4* cHT, cKO, and gHT mouse models and respective controls. All statistical analyses are via One-way ANOVA with Tukey's post-hoc test (*Emx1-Cre line*) or unpaired Student's t-test (*CMV-Cre line*). * $p < 0.05$. Biological n = 4 (WT-*Emx1*), 3 (cHT), 4 (cKO), 3 (WT-*CMV*), and 3 (gHT).

Chapter 4. Characterizing behaviour of *Chd4* mouse models

While *Chd4* mutants exhibited defects in cortical growth and cell composition, it remained unclear whether these defects affected cognitive function. We therefore sought to investigate changes in behaviour of our animal models. We ran the mice through a battery of behaviour tests in order to determine whether our models succeeded in recapitulating meaningful SIHIWES and related NDD phenotypes. Our battery of tests included assessing for learning and memory (Morris water maze test); assessing fear/anxiety (the elevated plus maze, open field test); assessing repetitive behaviours (the marble burying task); assessing sociability (adult social interaction test); and assessing for motor behaviour and sensorimotor coordination (rotarod test and beam break test). We chose to continue assessing *CMV-Cre* and *Emx1-Cre* lines separately due to significant differences in behaviour of the control mice (see control lanes in Figure 4.9 B/E, D/G; Figure 4.11B/G, C/H, D/I; Figure 4.12B/D for examples). These changes are most likely due to genetic drift during breeding. We also chose to pool male and female data together as we did not find significant differences between sexes in most test parameters. In instances where there were significant differences, sex-specific data is presented. Curiously, the *Chd4* cHTs, cKOs and gHTs all exhibit separate behavioural profiles, which also appear to be influenced at times by sex. The behaviour profiles of each model are summarized in Table 5.

Using the beam break test, we were able to assess baseline ambulatory activity over the course of 24 hours. Unfortunately, some data was lost due to a software malfunction, and only two *Chd4* cKO mice were able to be examined during the first three hours of testing. Despite this, we found all three mouse models exhibited fairly normal ambulatory activity (Figure 4.7A, B). Additionally, in order to confirm that our *Chd4* didn't have any visual impairments (which might

affect e.g. open field test and Morris Water Maze) we performed optomotor analysis (Supplementary Figure 2). No changes in visual acuity were observed. This suggests that our mouse models exhibit fairly normal baseline activity and vision.

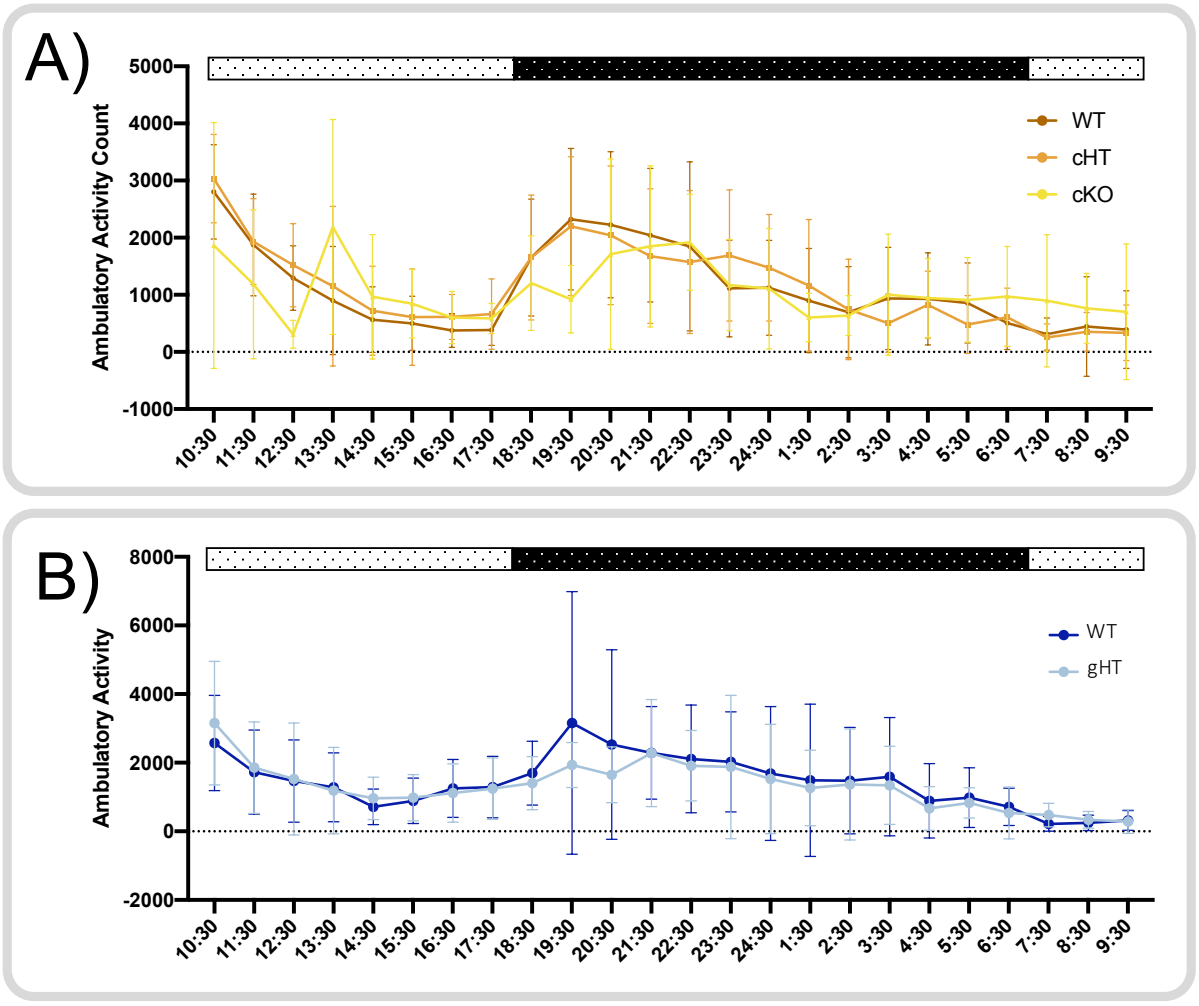

Figure 4.7. *Chd4* cHT, cKO and gHT mouse models present normal baseline activity on beam break test. A) Cumulative ambulatory activity counts per hour during the beam break test of WT *Chd4* cHT and *Chd4* cKO mice. **B)** Cumulative ambulatory activity counts per hour during the beam break test of WT and *Chd4* gHT mice. All mice were placed into testing apparatus at ~10:30 during the light cycle, as indicated in the bar above the graph (black = dark, white = light). Biological n = 32 (WT-*Emx1*, 19♂: 13♀), 15 (cHT, 9♂: 6♀), 6 (cKO, 3♂: 3♀), 26 (WT-*CMV*, 13♂: 13♀), and 16 (gHT, 8♂: 6♀).

In the open field test, mice are placed in the center of a field under a very bright light (Figure 4.8A). Mice tend to avoid this area with the bright light and preferentially stay in the corners. No changes were observed on this test for *Chd4* cHTs (Figure 4.8B-F) or *Chd4* gHTs (Figure 4.8G-J). Conversely, *Chd4* cKOs exhibited decreased velocity specifically in the first minute of the open field test (Figure 4.8F), and this lack of movement accounted for increased time spent in center of the field (Figure 4.8B), and increased latency before reaching the field corners (Figure 4.8D). After the initial minute, they appear to adapt and exhibit similar velocity and behaviour to WT mice. This suggests that *Chd4* cKOs may exhibit freezing or delayed reactions when first introduced into the new environment under the stress of bright lighting, and suggests an anxiety phenotype.

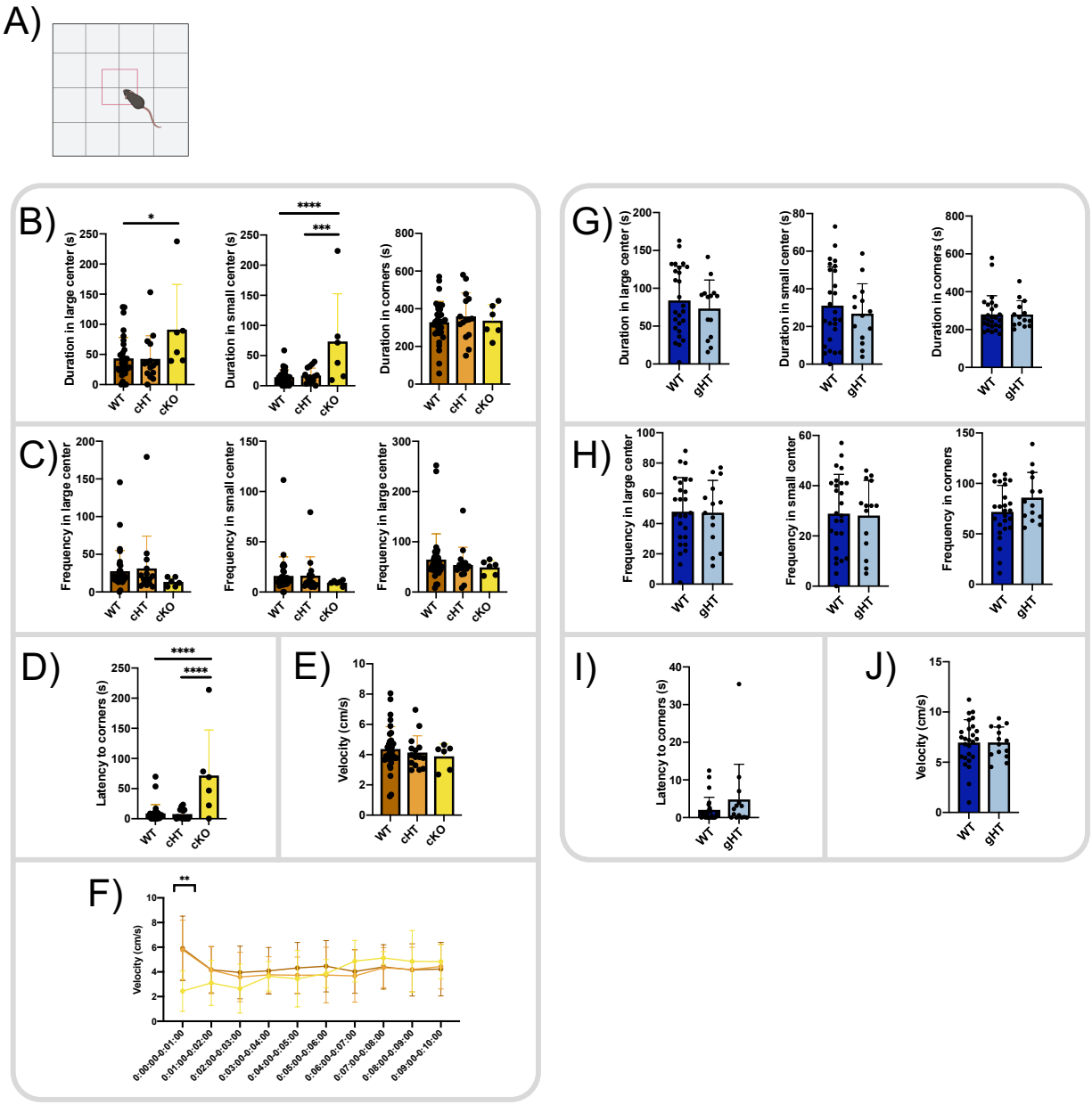

Figure 4.8. *Chd4* cKOs exhibit delayed reaction when placed inside the open field test. A) Sample schematic of the open field test. Created with BioRender.com. **B-C)** total cumulative duration in (B) and total number of times entering (C) the large center (left), small center (middle), and corners (right) of the open field test for WT, *Chd4* cHT and *Chd4* cKO mice. **D)** Latency to corners in the open field test for WT, *Chd4* cHT and *Chd4* cKO mice. **E)** Velocity of WT, *Chd4* cHT and *Chd4* cKO mice during open field test. **F)** Velocity per minute of WT, *Chd4* cHT and *Chd4* cKO mice during open field test. **G-H)**

total cumulative duration in (B) and total number of times entering (C) the large center (left), small center (middle), and corners (right) of the open field test for WT and gHT mice. **I)** Latency to corners in the open field test for WT and gHT mice. **J)** Velocity of WT and *Chd4* gHT mice during open field test. All statistical analyses are via One-way ANOVA with Tukey's post-hoc test (*Emx1-Cre line*) or unpaired Student's t-test (*CMV-Cre line*). * $p < 0.05$. *** $p < 0.001$. **** $p < 0.0001$. Biological n = 32 (WT-*Emx1*, 19♂: 13♀), 15 (cHT, 9♂: 6♀), 6 (cKO, 3♂: 3♀), 26 (WT-*CMV*, 13♂: 13♀), and 14 (gHT, 8♂: 6♀).

In the elevated plus maze, mice are placed in an elevated cross maze with two open arms and two enclosed arms (Figure 4.9A). As was the case for the elevated plus maze, neither *Chd4* cHT (Figure 4.9B-D) or *Chd4* gHTs (Figure 4.9E-G) displayed any variation during this test. However, *Chd4* cKOs spent less time in the central zone of the elevated plus maze, without affecting other parameters (Figure 4.9B). This may suggest that the mice take less time deciding which new arm to enter (i.e. variations in decision making behaviour), or that they are more averse to the being in the open center of the maze. Indeed, another mouse model with this phenotype was described as having increased anxiety, as the mice avoided an open portion (i.e. the center) of the maze[117]. Together, the data from the elevated plus maze and open field tests suggest that ablation of *Chd4* expression in the cortex can contribute towards anxiety behaviours in mice. Partial loss of *Chd4* expression (i.e. *Chd4* cHTs and gHTs) however, was not sufficient to cause the same phenotype.

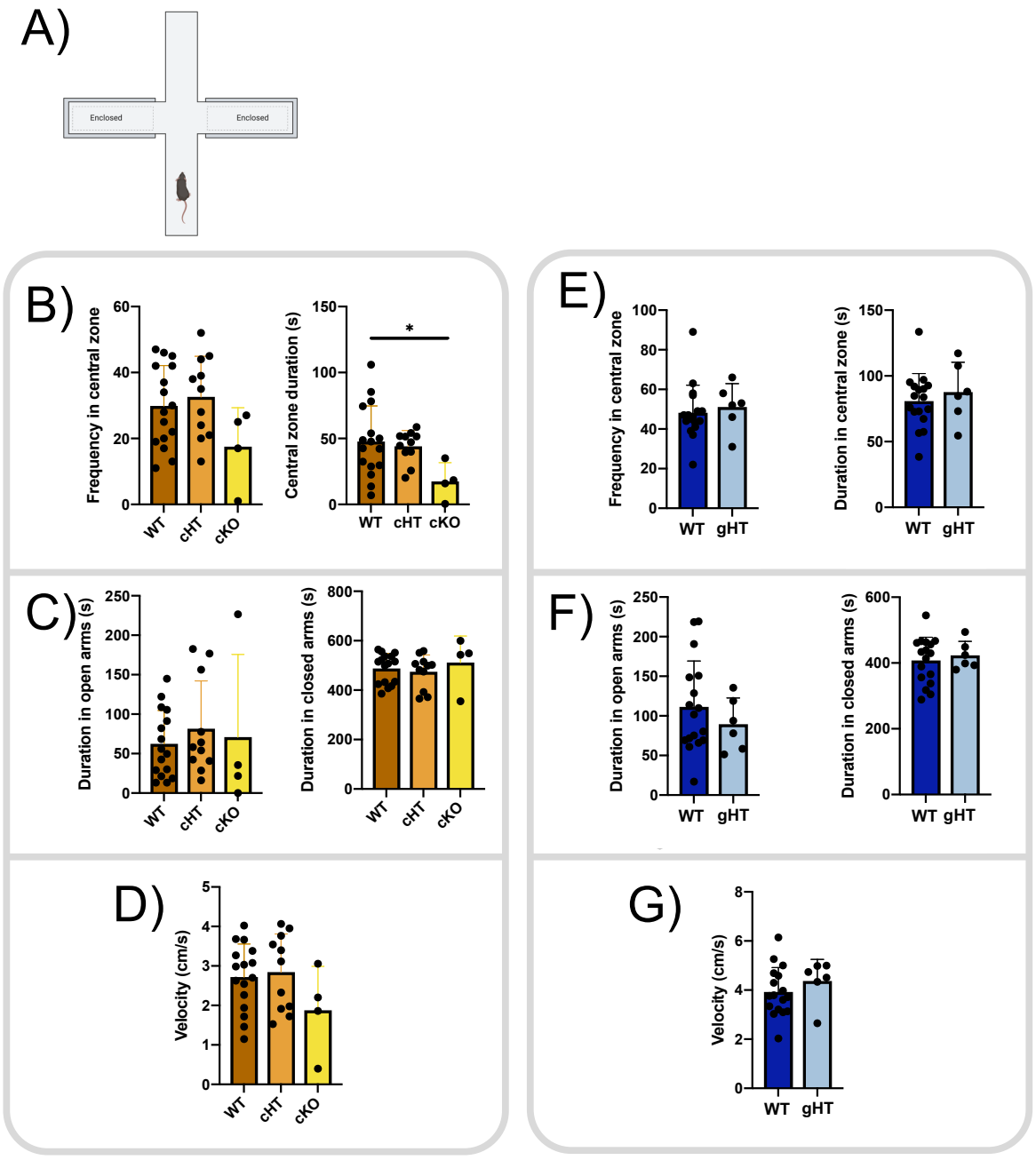

Figure 4.9. *Chd4* cKOs spend less time in the center zone of the elevated plus maze. A) Sample schematic of elevated plus maze. Created with BioRender.com. **B)** Number of times entering the central zone (left), total cumulative duration in the center zone (right), **C)** Total cumulative duration in open arms (left), total cumulative duration in closed arms (right), and **D)** velocity of WT, *Chd4* cHT and *Chd4* cKO mice in the elevated plus maze. **E)** Number of times entering the central zone (left), total cumulative

duration in the center zone (right), **F)** Total cumulative duration in open arms (left), total cumulative duration in closed arms (right), and **G)** velocity of WT and *Chd4* gHT mice in the elevated plus maze. All statistical analyses are via One-way ANOVA with Tukey's post-hoc test (*Emx1-Cre line*) or unpaired Student's t-test (*CMV-Cre line*). * $p < 0.05$. Biological n = 16 (WT-*Emx1*, 10♂: 6♀), 11 (cHT, 5♂: 6♀), 4 (cKO, 1♂: 3♀), 17 (WT-*CMV*, 12♂: 5♀), and 13 (gHT, 5♂: 1♀).

During the marble burying test, mice are placed into a cage with 20 evenly spaced marbles (Figure 4.10A). The number of marbles mice bury after half an hour is used as an indication of repetitive behaviours. We found that *Chd4* cHTs buried significantly more marbles compared to WT (Figure 4.10B). This suggests that *Chd4* cHTs exhibit increased repetitive behaviours. *Chd4* cKOs appeared to exhibit a dichotomy in terms of their behaviour. Nearly all the marbles seemed to be buried, or none at all (Figure 4.10B). When separated by sex, females seem to bury none of the marbles (Figure 4.10D), though as the sample size is small, it is possible that this result is simply due to undersampling. As we have previously observed *Chd4* cKOs exhibiting anxiety-like behaviours in the elevated plus maze and the open field test, it is possible that the introduction into this testing environment may also result in an anxiety phenotype, affecting their behaviour. For instance, they may have an aversion to new foreign objects (e.g. marbles) or, be less aware of them. However, it appears that in the event *Chd4* cKOs do bury marbles, they present with increased repetitive movements like the *Chd4* cHTs. Full body *Chd4* gHTs did not exhibit any changes in marble burying (Figure 4.10E, F).

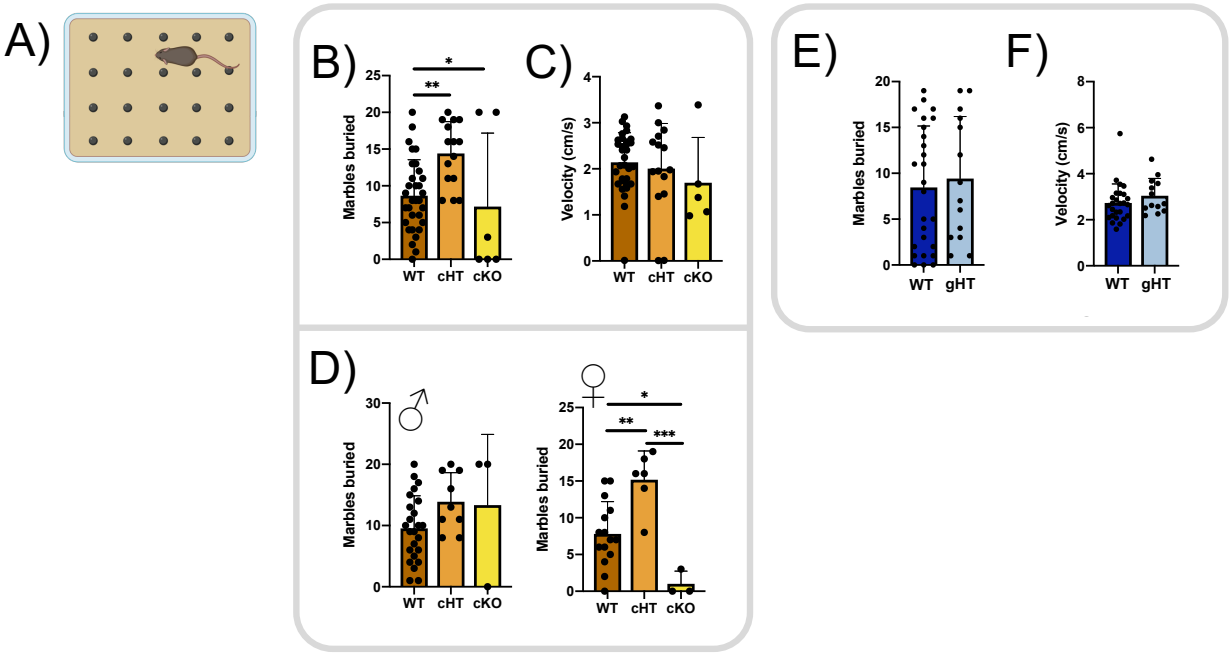

Figure 4.10. *Chd4* cHTs exhibit increased repetitive movements in marble burying test. A) Sample schematic of the marble burying test. Created with BioRender.com. **B)** Total number of marbles by *Chd4* WT, cHT and cKO mice. **C)** Velocity of *Chd4* WT, cHT and cKO mice during testing. **D)** Total number of marbles by male (left) and female (right) *Chd4* WT, cHT and cKO mice. **E)** Total number of marbles by control WT and *Chd4* gHT mice. **C)** Velocity of WT and *Chd4* gHT mice during testing. All statistical analyses are via One-way ANOVA with Tukey's post-hoc test (*Emx1-Cre line*) or unpaired Student's t-test (*CMV-Cre line*). * $p < 0.05$. ** $p < 0.01$. *** $p < 0.001$. Biological n = 32 (WT-*Emx1*, 19♂: 13♀), 15 (cHT, 9♂: 6♀), 6 (cKO, 3♂: 3♀), 26 (WT-*CMV*, 13♂: 13♀), and 14 (gHT, 8♂: 6♀).

During the adult social interaction test, a mouse is first habituated to a chamber with an empty cage, and subsequently reintroduced into the chamber with a stranger mouse in the cage (Figure 4.11A - schematic of socialization phase). *Chd4* cHTs exhibited increased frequency of times spent entering the large interaction zone around the stranger mouse during the socialization period compared to wildtype, but not during the habituation phase (Figure 4.11C frequency in large interaction zone). However, duration of time spent in the large interaction zone (Figure 4.11B) and velocity during the socialization phase (Figure 4.11D) remained unchanged. From this, we deduced that *Chd4* cHTs visit the stranger mouse more frequently but stay for briefer periods of time, while control mice visit the stranger mice less frequently but stay in the interaction zone for longer amounts of time. We were able to confirm this finding by inspecting video footage. Hence, *Chd4* cHTs present with a variation in socialization behaviour. *Chd4* cKOs also presented with a change in behaviour during the adult social interaction test, however it differed from *Chd4* cHTs. *Chd4* cKOs spent less time in socialization areas and entered the socialization areas less frequently during the habituation and socialization phases (Figure 4.11B, C). There was also a decrease in velocity during the habituation and socialization periods of this test (Figure 4.11D). Curiously, unlike the open field test where velocity is only decreased during the first minute, decreased velocity is maintained throughout testing in the ASI test (Figure 4.11 F). Moreover, this decrease is not reflected in velocity measurements from other tests (e.g. open field test, Figure 4.8E; marble burying test, Figure 4.10C). This suggests that the environment of this particular test affected the mice in such a way that they slowed down and/or were more hesitant to explore the empty cage and/or stranger mice. Of note, the ASI test is the only test included that was performed in the dark, which may have influenced behaviour. Additionally, upon outlier removal (red star), the ratio of time the mice spent in the large and small interaction

zones during the socialization period compared to the habituation period was not significantly different (Figure 4.11E), further suggesting that the cKO phenotype manifests due to the environment and not the socialization aspect of this test. On the other hand, *Chd4* gHT mice did not exhibit any changes in socialization during the ASI test (Figure 4.11G-J). Thus, telencephalon-specific loss or ablation of Chd4 alters socialization behaviour, while full body loss did not.

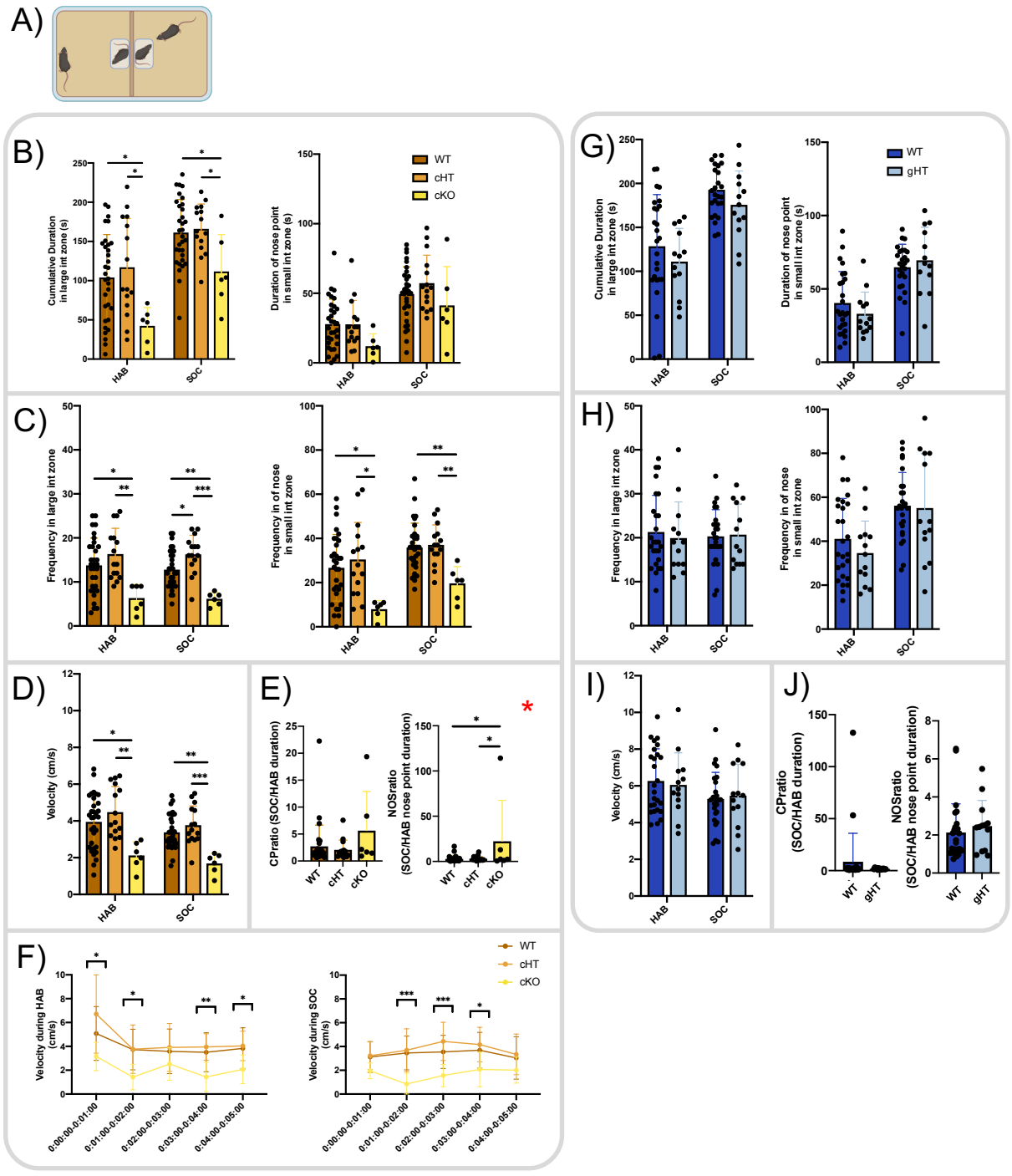

Figure 4.11. ***Chd4*** **cHT and cKO present with altered behaviours during the adult social interaction test. A)** Sample schematic of two independent trials of the adult social interaction test occurring simultaneously (social phase). During the habituation phase, both cages inside the field containing mice are empty. Created with BioRender.com. **B)** Total cumulative duration WT, *Chd4* cHT and *Chd4* cKO

mice spend in the large interaction zone (left) and total cumulative duration their noses spend in the small interaction zone (right) during habituation (HAB) and social (SOC) trials. **C)** Total number of times WT, *Chd4* cHT and *Chd4* cKO mice enter the large interaction zone (left) and total number of times their noses enter the small interaction zone (right) during habituation (HAB) and social (SOC) trials. **D)** Velocity of WT, *Chd4* cHT and *Chd4* cKO mice during testing. **E)** Ratio of time WT, *Chd4* cHT and *Chd4* cKO mice spend in large interaction zone during the social versus the habituation phase (left) and ratio of time the mice's noses spend in small interaction zone during the social versus the habituation phase (right). **F)** Velocity per minute of WT, *Chd4* cHT and *Chd4* cKO mice during testing. **G)** Total cumulative duration WT and *Chd4* gHT mice spend in the large interaction zone (left) and total cumulative duration their noses spend in the small interaction zone (right) during habituation (HAB) and social (SOC) trials. **H)** Total number of times WT, and *Chd4* gHT mice enter the large interaction zone (left) and total number of times their noses enter the small interaction zone (right) during habituation (HAB) and social (SOC) trials. **I)** Velocity of WT and *Chd4* gHT mice during testing. **J)** Ratio of time WT and *Chd4* gHT mice spend in large interaction zone during the social versus the habituation phase (left) and ratio of time the mice's noses spend in small interaction zone during the social versus the habituation phase. All statistical analyses are via One-way ANOVA with Tukey's post-hoc test (*Emx1-Cre line*) or unpaired Student's t-test (*CMV-Cre line*). * $p < 0.05$. ** $p < 0.01$. *** $p < 0.001$. Biological n = 32 (WT-*Emx1*, 19♂: 13♀), 15 (cHT, 9♂: 6♀), 6 (cKO, 3♂: 3♀), 26 (WT-*CMV*, 13♂: 13♀), and 13 (gHT, 8♂: 5♀).

The Morris Water Maze test was used to assess for changes in spatial learning and memory, which may recapitulate learning aspects of ID. In this test, mice are trained over the course of 6 days to find a platform based on visual cues (Figure 4.12A). On the 7th day (probe day) the platform is removed and the ability of the mice to remember the platform's location is tested. *Chd4* gHT mice take longer to find the platform on Day 3 than WT mice (Figure 4.7E), and there is a consistent trend of this happening throughout training. This seems to be especially noticeable in female gHT mice (Figure 4.7G). Additionally, female *Chd4* gHT mice have significantly decreased frequency of crossing the platform area on probe day (Figure 4.7G). Conversely, neither *Chd4* cHTs or cKOs presented with significant changes in learning and memory during the Morris Water Maze test (Figure 4.7B). Therefore, only the Chd4 gHT mouse models, especially females of this model, presented with impaired spatial learning and memory.

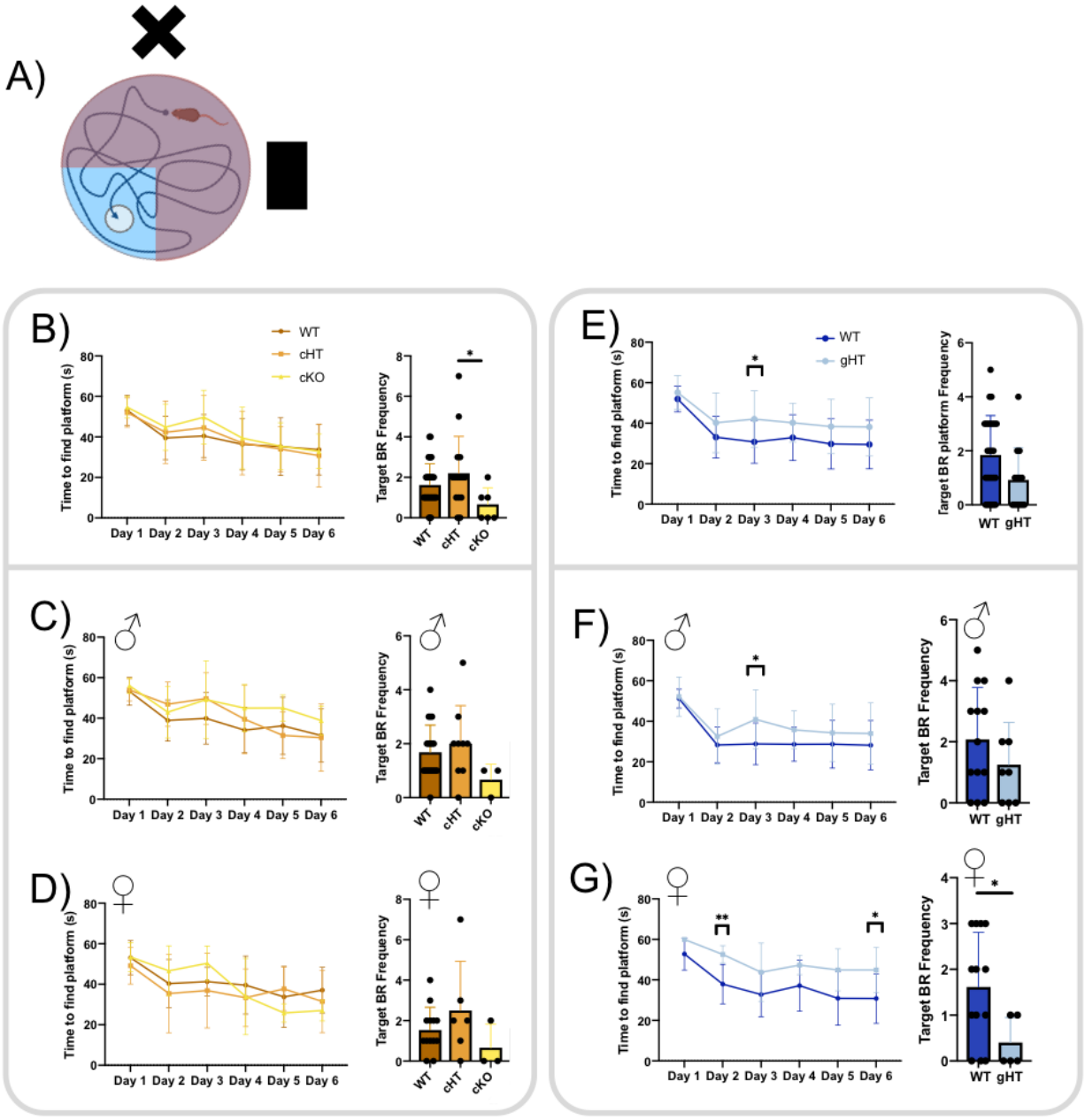

Figure 4.12. Female *Chd4* gHT exhibit impaired learning and memory in the Morris Water Maze test. A) Sample schematic of Morris Water Maze. Black cross and black rectangle represent visual cues to located the position of the hidden platform. Created with BioRender.com. **B-D)** Time to find the platform during Morris Water Maze training (left) and frequency of crossing platform area during probe day (right) for all mice (B), male mice (C) and female mice (D) of WTs, *Chd4* cHTs and *Chd4* cKOs. **E-G)** Time to find the platform during Morris Water Maze training (left) and frequency of crossing platform area during

probe day (right) for all mice (E), male mice (F) and female mice (G) of WT and *Chd4* gHTs. All statistical analyses are via One-way ANOVA with Tukey's post-hoc test (*Emx1-Cre line*) or unpaired Student's t-test (*CMV-Cre line*). * $p < 0.05$. ** $p < 0.01$. Biological n = 32 (WT-*Emx1*, 19♂: 13♀), 15 (cHT, 9♂: 6♀), 6 (cKO, 3♂: 3♀), 26 (WT-*CMV*, 13♂: 13♀), and 13 (gHT, 8♂: 5♀).

Impaired spatial learning in female *Chd4* gHTs was further implicated in the rotarod test. The rotarod test trains mice over the course of four days to stay on a rod that incrementally increases its rotation speed, allowing for assessment of motor coordination and movement (Figure 4.12A). Neither *Chd4* cHTs, cKOs or male gHTS displayed any changes in motor function (Figure 4.12B, E). However, we found that female *Chd4* gHT mice had a decreased latency to fall during Day 3 and Day 4 of rotarod training (Figure 4.12E). To test whether this was the result of difficulty learning or of rotarod-specific impaired motor activity, we performed a preliminary 10-day training rotarod test on a small group of female mice. We found that the tested female *Chd4* gHTs could improve over time and were able to stay on the rotarod for the full length of time during certain trials (Figure 4.12F). This suggests that, as in the Morris Water Maze, female *Chd4* gHTs may present with impaired learning on this test. Future research can be done to better examine this. As male *Chd4* gHT mice do not show this phenotype, it also suggests a sex specific effect.

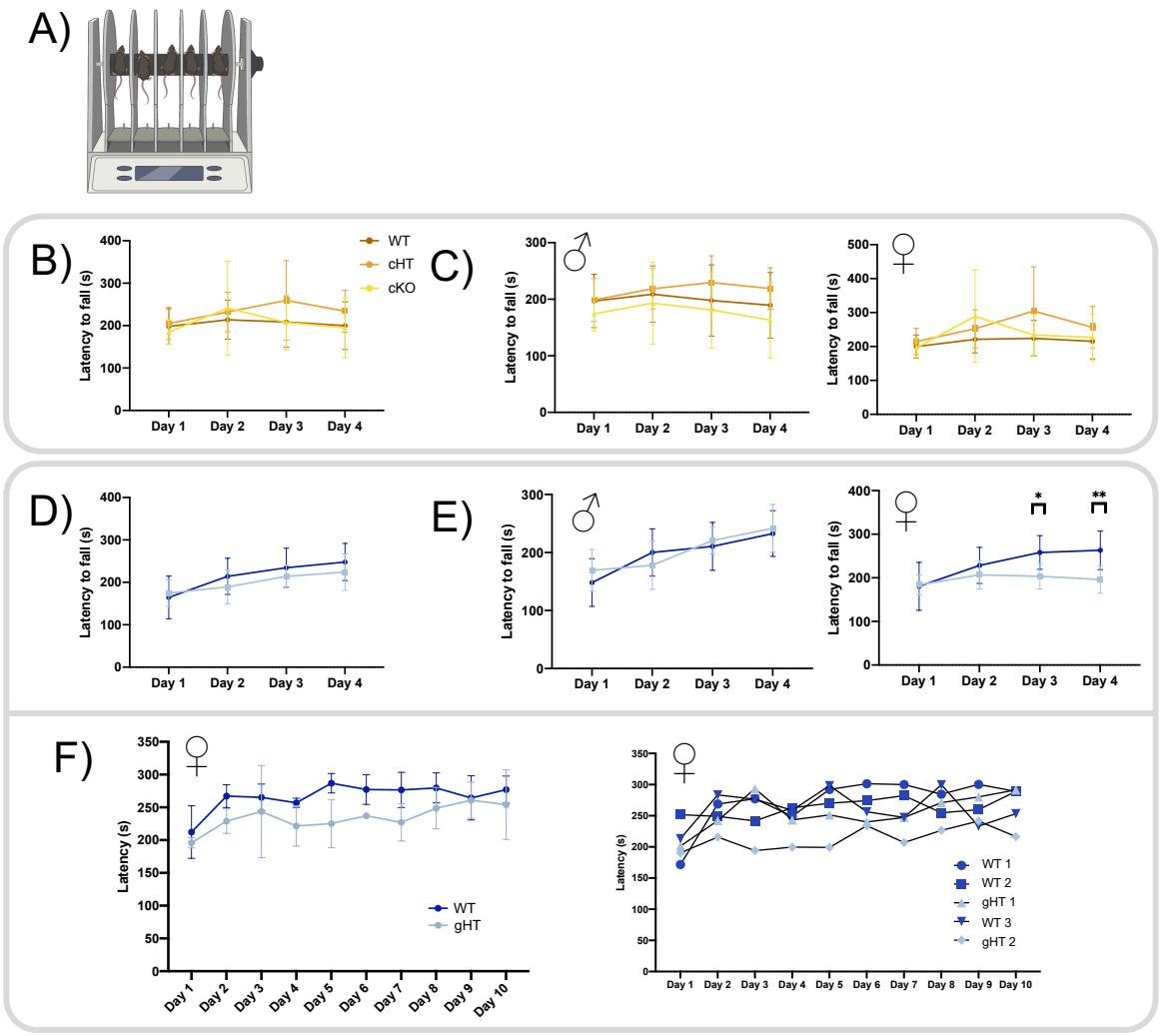

Figure 4.13. Female *Chd4* gHTs present with impaired learning during the rotarod test. A) Sample schematic of the accelerating rotarod test, performed for four consecutive days with four five-minute trials per day. Created with BioRender.com. **B-C)** Latency of fall of rotarod for all (B), male (C, left), and female (C, right) WT, *Chd4* cHT and *Chd4* cKO mice. **D-E)** Latency of fall of rotarod for all (B), male (C, left), and female (C, right) WT and *Chd4* gHT mice. **F)** The accelerating rotarod test was performed over the course of ten consecutive days with four five-minute trials per day. Data grouped by WT and gHT genotype (left) versus individual mouse plots (left) are shown. All statistical analyses are via One-way ANOVA with Tukey's post-hoc test (*Emx1-Cre line*) or unpaired Student's t-test (*CMV-Cre line*). * $p < 0.05$. ** $p < 0.01$. Biological n = 32 (WT-*Emx1*, 19♂: 13♀), 15 (cHT, 9♂: 6♀), 6 (cKO, 3♂: 3♀), 26 (WT-*CMV*, 13♂: 13♀), and 13 (gHT, 8♂: 5♀).

Overall, each *Chd4* mouse model presents with a different subset of behaviours which are very likely dependent on how and where *Chd4* expression is altered. Changes in anxiety, sociality and repetitive movements were only present when the cortex was targeted (*Chd4* cHT, cKO), while changes in learning behaviours were only observed when the whole-body was targeted (*Chd4* gHT), especially in the case of female mice. Additionally, behaviour phenotypes appeared more severely affected when *Chd4* was ablated (cKO) versus partial loss of *Chd4* expression (cHT). A summary of observed behaviour phenotypes is found in Table 5.

Table 5. Summary of *Chd4* cHT, cKO and gHT mouse model observed phenotypes.

SIHIWES mouse model	Gross Anatomy	Immunohistochemistry	Behaviour
 *(Emx1-Cre) Chd4 cHT*	❖ ↑ WM thickness	❖ ↑ Olig2+ cells (bin 1)	REPETIVITVE MOVEMENTS ❖ ↑ repetitive movements (marble) ❖ ↑ frequency in large IZ (ASI)
 *(Emx1-Cre) Chd4 cKO*	❖ ↓ observed # (Mendelian) ❖ ↓ brain weight ❖ ↓ cortex area ❖ ↓ cortex thickness ❖ ↓ WM thickness	❖ ↓ Hoechst+ cells (total) ❖ ↓ Brn2+ cells (total; upper bins) ❖ ↓ Satb2+ cells (total; upper bins)	ANXIETY/FEAR BEHAVIOURS ❖ ↑ duration in center (OF) ❖ ↑ latency to corners (OF) ❖ ↓ central zone duration (EPM) ❖ △ repetitive movements (marble) ❖ ↓ Velocity & △ behaviour (ASI)
 *(CMV-Cre) Chd4 gHT*	❖ ↓ cortex area	❖ ↓ Ctip2+ cells (total)	LEARNING & MEMORY ❖ ↓ learning (WMW) ❖ ♀ ↓ learning & memory (MWM) ❖ ♀ ↓ learning? (rotarod)

Created with BioRender.com

Chapter 5. Discussion

We showed that *Chd4* is expressed in diverse neural cells within the developing cortex. We were additionally able to produce and examine three viable mouse models of *Chd4* syndrome, allowing for investigation of postnatal brain development and behavior, and extending the work of mouse models previously examined embryonically. The three models presented with unique profiles in terms of gross anatomy, cell composition and behaviour, summarized in Table 5 and explained more in depth below.

5.1 Cortical development in genetic mouse models of SIHIWES

We were able to successfully build upon previous research in *Chd4* cKO neonates by developing the first *Chd4* cKO mouse model that can be examined postnally. It appears that although *Chd4* is essential for life (*Chd4* germline KOs are lethal[108]), and essential in the brain for survival postnally (*Nestin-Cre Chd4* cKOs are perinatally lethal[84]), mice with loss of *Chd4* expression in the dorsal telencephalon are viable, though recovered less frequently than expected. At least one *Chd4* cKO animal was also lost to hydrocephalus, a symptom associated with SIHIWES, and not included in the analysis. It remains unclear whether this phenotype was true to the *Chd4* cKOs or whether it arose spontaneously in the colony.

The cortex of *Chd4* cKOs was smaller, encompassing decreased brain weight, area of the cortex, thickness of the cortex and decreased thickness of white matter under the cortex. Notably, as expected, cerebellum area did not change, suggesting that growth defects were autonomous to the telencephalon. Histological analysis revealed this was largely due to a decrease in upper layer markers Satb2 and Brn2. The observed phenotype of *Chd4* cKOs phenotype is consistent with

previously developed *Nestin-Cre Chd4* cKO models by Nitarska et al[84]. These *Nestin-Cre Chd4* cKOs also presented decreased brain size that appears to be mostly due to a decrease specific to upper layer neurons. Further investigations revealed that this was due to impaired proliferation of the progenitor cells and increased cell death of apical and intermediate progenitor cells. Hence, the decreased upper layer markers in our *Chd4* cKO model is likely also explained by these phenomena. Additionally, *Chd4* cKOs presented with an increase in Ctip2 Brn2 double positive cells. More will need to be done to determine the exact nature of these double positive cells, whether they are a naturally occurring subtype whose population became expanded, or cells that struggle to adopt a final layer identity. Interestingly, conditional knockout of the NuRD complex subunit *Mbd3* has been reported to cause misexpression of both deep and upper layer markers in cortical neurons[118].

Chd4 cHTs showed no signs of decreased brain weight or cortex area. In fact, they had increased thickness of white matter in coronal sections of the cortex, and a slight increase of Olig2+ cells in the upper area of the cortex. Changes in white matter are frequently observed in neurodevelopmental syndromes, including ASD and a subset of SIHIWES cases[62,119,120]. Additionally, triplication of *Olig1* and *Olig2* genes in human Down syndrome neural progenitor cells[121] and in certain mouse models of Down syndrome[122] leads to overexpression and concomitant overproduction of oligodendroglial cells. Moreover, studies have linked *Olig* genes to the associated neurodevelopmental cognitive symptoms of Down syndrome[121-124] and Olig2's importance during in neurodevelopment has been extensively reported (reviewed here[125]). Future work can be done to fully characterize changes in white matter within the *Chd4* cHT. This may

include looking at larger white matter structures and investigating the projection patterns of cortical neurons.

Interesting, *Chd4* gHTs presented with decreased brain weight and cortex area, similarly to *Chd4* cKOs. As *Chd4* cHT didn't present with this phenotype, it suggests that *Chd4* plays a key role in cortical development, prior to E9.5 (the onset of *Emx1* expression). Moreover, as cerebellum area and body weight were unaffected in *Chd4* gHTs, it suggests that this early role may still be specific to the telencephalon, although other subcortical structures we didn't examine might also be affected. Moreover, this mechanism is independent to that observed in *Chd4* cKOs, where *Chd4* expression is lost only after E9.5. Supporting this, *Chd4* gHTs had lesser reductions in cortical area versus *Chd4* cKOs, and cortical thickness was unaffected. *Chd4* gHTs also did not present with a deficit in upper layer neurons. This provides evidence that haploinsufficiency of *Chd4* in very early stages is sufficient to have an effect on cortical development. This also correlates well with the literature, as haploinsufficiency of several CHD members and other chromatin remodelers can be lethal and/or lead to NDDs[66,126-128]. *Chd4* gHTs also presented with a decreased number of Ctip2+ neurons, which might suggest a specific requirement for Chd4 in these cells. Indeed, Tbr1, another deep layer marker, did not change. Moreover, Ctip2 and Ctip factors have been shown to interact with the NuRD complex[96,97,129]. As Ctip2 is also a layer V determinant transcription factor, its misexpression can have a direct impact on the specification of layer-specific identities[130]. Future work will need to be done to fully characterize this phenotype.

5.2 Behavioural variations in genetic mouse models of SIHIWES

Our SIHIWES mouse models demonstrated that variants of *Chd4* can cause changes in both cortical growth and in behaviour. Moreover, behavioural changes could be observed even when *Chd4* was only decreased or conditionally ablated from the cortex. Though there is still work to be done, these findings provide significant weight towards linking cortex specific structural changes (due to variations in chromatin remodelling) to alterations in behaviours, as well as providing models to investigate the involved mechanisms.

In addition to generating the first viable *Chd4* cKO in the cortex, we also were able to generate the first *Chd4* cKO mice able to be assessed behaviourally. *Chd4* cKOs presented with decreased velocity/freezing behaviour during the first minute of the open field test, a decreased amount of time spent in the center zone of the elevated plus maze, tendencies towards burying all or none of the marbles, and decreased velocity throughout the adult social interaction test. Interestingly, it has been previously reported that several genetic mouse models of ASD take longer time to evaluate and respond to visual threats[131]. These findings might correspond to the observed phenotype of our *Chd4* cKOs in the open field test; they take longer to respond to the bright light visual cue, demonstrated by their delay to move into the corners of the field and decreased velocity at the beginning of the test. Meanwhile, increased repetitive behaviours are a frequent hallmark of NDDs including ASD and OCD[132-134]. It is interesting that some of our *Chd4* cKOs show tendencies towards increased repetitive movements, like the *Chd4* cHTs, while others do not bury any of the marbles. Moreover, decreased marble burying has been previously observed in another mouse model of ASD, involving the knockout of the excitatory postsynaptic metabotropic glutamate receptor 5 (mGluR5)[135]. Looking towards the EPM test, it is possible

that elevated anxiety might drive an aversion towards foreign objects. Changes in behaviour during ASI testing are also frequent in mouse models of ASD, with, for example, the mGluR5 model reporting decreased velocity in a subset of tests as well[135].

Chd4 cHTs presented with increased repetitive movements (marble burying test) and variation in social behaviour during the adult social interaction test. As mentioned above, increased repetitive behaviours are frequently noted in individuals with neurodevelopmental conditions, including autism spectrum disorder, obsessive compulsive disorder (OCD), and Down Syndrome, and in mouse models of these conditions[132-134]. Changes in social behaviours are often observed in neurodevelopmental conditions like ASD and mouse models of ASD too[136].

Chd4 gHTs exhibited behaviours that were generally indistinguishable from control mice. However female *Chd4* gHTs exhibited decreased spatial learning and memory during the Morris Water Maze test. Learning deficits also appeared to occur during the rotarod test. Notably, body weight can affect performance on the rotarod test, and as *Chd4* gHT trend towards decreased body weight, it may have been a confounding factor for the latter observations[137]. However, mobility and velocity of the mice was not impaired in any other tests including Morris Water Maze. Learning and memory are affected in human ID, a hallmark symptom of SIHIWES, so our results suggest that female *Chd4* gHTs may recapitulate an aspect of this phenotype. A comparison between these gHT phenotypes versus the lack of equivalent deficits in cHT females suggests that *Chd4* is required in cells derived outside of cortical lineages. Indeed, mice with a conditional knockout of *Chd4* in the cerebellum had impacted learning on the rotarod as well[111], with gait and motor activity otherwise unaffected. This may suggest that *Chd4* haploinsufficiency is sufficient to drive certain learning impairments.

5.3 Comparing genetic mouse models of SIHIWES

Examining the similarities and differences between our models gives us clues towards where *Chd4* may be most important. Interestingly, *Chd4* cHT and cKO tended to follow opposing trends in terms of thickness of the cortex, white matter layer thickness, and total cell number in somatosensory cortex, highlighting how conditional heterozygous versus knockout loss of Chd4 may affect brain development in diverging ways. In all other aspects, unsurprisingly, increased loss of *Chd4* resulted in more severe observed phenotypes, with *Chd4* cHT being the least affected, followed by gHT, and then cKO, which presented with the most blatant changes. Accordingly, behavioural tests that yielded *Chd4* cHT phenotypes also yielded phenotypes in *Chd4* cKOs and were often more overt. Partial loss of *Chd4* (cHT) was sufficient to affect some social and repetitive movement behaviours, however only ablation of Chd4 (cKO) was sufficient to induce observable anxiety phenotypes.

Interestingly, our *Chd4* gHT mice did not display the aforementioned changes in repetitive movement and social behaviours that the *Chd4* cHT displayed. Further investigations may need to be done in order to examine why this is. One potential avenue to explore is focusing on the role of *Chd4* in neurons. Work in the cerebellum demonstrates that *Chd4* can play important roles in post mitotic neurons[110-112]. And while *Chd4* gHT mice have both inhibitory and excitatory neurons of the cortex targeted for reduction of *Chd4*, *Chd4* cHTs and cKOs only have targeted loss in excitatory neurons. This could lead to imbalances in the cortical excitatory vs inhibitory circuitry, which has been highlighted as a strong cause of ASD[138]. Alternatively, it is possible that the *Chd4* gHTs have less behaviour phenotypes because they had more time to develop and activate compensating mechanisms, as *Chd4* expression is impacted at an earlier

time point. Indeed, some CHD subunits have been shown to partially compensate for each other[84].

We observe a sex difference in terms of learning and memory in our *Chd4* gHTs, with females being more affected than males. It is unclear why females would be more affected in our model, though sex-specific changes in learning behaviours of rodents have previously been reported[139,140]. It is possible that these behaviour changes might be correlated to a sex-specific cortical growth defects (i.e. decreased brain weight and cortex area), which we have yet to examine. Future research can help further unpack the mechanism behind this sex-specific difference in mice. The current identified cohort of SIHIWES cases only includes 12 females and 20 males, making it hard to draw conclusions regarding sex-specific differences in humans. Future work might also reveal whether females are actually more severely impacted. Historically, males have been diagnosed with NDDs (e.g. ASD, ADHD) more than females, which has been linked the existence of several X-linked conditions. Though the diagnosis criteria used to capture affected individuals has also been recently highlighted as a contributing factor[7-9].

Fascinatingly, this work reflects something observed in humans; variants in the same gene can lead to differing phenotypes. Specifically, changing the level or restriction pattern of a mutated gene can lead to diversity in phenotypes. In humans, this may be analogous to how each individual has a different set of unique variants, all with various degrees of impact, alongside *CHD4* that culminate together to yield a unique phenotype. Moreover, the effect of sensitizing alleles has been demonstrated in mice, wherein different mouse models of *CHD8* syndrome resulted in varying phenotypes depending on the strain (i.e. genetic background of the mice)

used[141]. Indeed, differences in genetic background may have also contributed towards the subtle differences observed between *Emx1-Cre* and *CMV-Cre lines* we used as well. Additionally, this work also reflected how a similar phenotype, i.e. decreased brain weight and cortex thickness, can be caused by different mechanisms (*Chd4* gHT vs cKO). And yet, the same basic processes are likely affected in each. Further investigations uncovering how changes at the genetic level led to these different observable phenotypes may be useful to understand affected chromatin remodeling mechanisms and identify treatment targets.

5.4 Understanding *Chd4's* relevance to neurodevelopment

Our work helped expand upon several gaps in the literature. 1) We were able to examine a postnatal *Chd4* cKO mouse models for changes in histology and behaviours. 2) We were able to characterize two *Chd4* heterozygote models, which more closely reflect SIHIWES variants, including predicted truncating variants. 3) We demonstrated that haploinsufficiency of *Chd4* was sufficient to affect cortical growth, neocortical neuron composition, and behaviour. 4) We did not observe cortical overgrowth or macrocephaly in our haploinsufficiency models, suggesting that this symptom might arise via other types of variants (e.g. specific point mutations, dominant-negative variants, variants that gains novel function, etc.) in humans. 5) We were able to demonstrate that *Chd4* mouse models are capable of exhibiting similar phenotypes through different mechanisms, as well as 6) having the same affected gene (*Chd4*) lead to unique phenotype profiles depending on when and where it was excised. We feel that this has advanced our understanding of how chromatin remodelling contributes to neurodevelopment and NDDs, which implications for understanding *CHD4* variants and likely extending into other NuRDopathies.

5.4 Limitations and Future Directions

Of course, there were limitations to our work that future research can expand upon. For instance, we were unable to fully examine how *Chd4* variants impact cortex development to cause changes in behaviour. Future work looking at cell expression (e.g. single cell RNA- sequencing), changes in chromatin accessibility (e.g. ATAC-seq), and functional assays of cortical neurons (e.g. patch-clamps recordings) of our *Chd4* mouse models may be especially helpful in doing so. This phenotyping could also help expand upon how chromatin remodelling is affected in the models, and how these impairments in turn drive the phenotypes. Moreover, white matter structures and structures outside the cortical cell lineage could also be further investigated. For example, a more thorough examination of white matter in the brain may help determine the phenotype of *Chd4* cHT. Additionally, the hippocampus of *Chd4* cKO mice was severely altered, with what appears to be complete loss of the dentate gyrus (Figure 3.2E). Despite this, *Chd4* cKOs exhibited no deficits in spatial learning and memory compared to wildtype mice (Figure 4.7B). This leaves an open area of investigation for hippocampus development and rewiring of the hippocampus to be researched.

Moreover, structures outside the cortex and hippocampus are likely affected in *Chd4* gHT, and could use further exploration. In fact, *CHD4* variants very likely may affect neurodevelopment by acting outside of neural lineages. For example, *de novo CHD4* variants have been implicated in a rare cerebrovascular disease called Moyamoya angiopathy (MMA), wherein stenosis of the distal internal carotid arteries leads to childhood-onset stroke and associated neurological impairments[142]. It is therefore possible that our *Chd4* mouse models could also experience

alterations in cerebral blood flow, affecting brain development and behaviour. *CHD4* variants are additionally associated with congenital heart disease and cancer, further highlighting potential associations that could also play a role in *Chd4* variant pathology.

Additionally, though we examined spatial learning and memory in our mouse models, it is possible that these mice exhibited behaviour phenotypes that were not captured by the scope of our testing. For example, fear conditioning tests, Barnes maze, or the IntelliCage, may have been more sensitive to other learning phenotypes. Moreover, it possible that the mild-moderate ID phenotype observed in humans does not translate well to mice.

Finally, we were unable to examine other potential variants of *CHD4* in SIHIWES. Our work supports the idea that human *CHD4* variants may act in a dominant negative fashion or gain a novel function to yield certain phenotypes including macrocephaly. Moreover, that mechanism would necessarily be different than that observed in our haploinsufficient mouse models, leaving another area open to explore. However, the diversity exhibited by our haploinsufficient models demonstrates that multiple variants may be necessary to fully understand SIHIWES pathologies. In the future, work can be expanded upon to create patient specific variants and examining them in animal models and functional assays. We hope extension of this work will allow for identification of underlying chromatin remodelling mechanisms leading to disadvantageous effects in individuals (e.g. intellectual disability, hydrocephalus, etc.), which can be therapeutically targeted. Moreover, we hope that this will permit subcategorization of NDDs based on the mechanistic causes, perhaps facilitating corresponding personalized treatment plans.

5.5 Conclusion

In conclusion, we successfully developed three novel mouse models of CHD4 syndrome that each presented with a unique profile of neurodevelopmental and behavioural features, some of which recapitulated SIHIWES phenotypes. This encompassed two heterozygote models, which better reflected patient genetics, and a novel, viable conditional *Chd4* knockout mouse. Our work suggests that *Chd4* variants in the cortex can affect both cortical development and behaviour, though *Chd4* mutations outside the cortex are likely responsible for changes in spatial learning and memory, and other variants may be more important in developing cortical overgrowth phenotypes. Our work underscores the importance of diversity even when a single gene is mutated, and the importance of the chromatin remodelling gene *Chd4* during neurodevelopment. Future work can help continue to unravel the affected pathways and mechanisms these variants play a role in to affect the developing brain.

Appendix

The following is a brief word on neurodiversity and language. According to the DMS-5, the term "neurodevelopmental disorders" refers towards a wide spectrum of conditions including autism spectrum disorders and ADHD, as has been used in this paper according to that definition. However, it has been argued that individuals with different neurocognitive parameters, including autistic individuals, are a part of the normal variation within society, and therefore not "disordered". Indeed, some NDD traits can be seen as advantageous in certain scenarios. This has led to the development of terminology including neurodiversity, neurodivergent and neurotypical, with the former first coined by Judy Singer in 1998[143]. This further brings into discussion whether socio-environmental models or medical models of treatments should come into play when addressing all individuals with these conditions. This is especially of note when considering the grand spectrum of severity the term NDD has come to encompass, and considering that there are certain NDDs, such as cases of fragile X syndrome, that fall outside of a "normal range" of impairment. In an attempt to unite viewpoints, Scotland's National Autism Implementation Team offered new definitions and models of these terms[144], which were not reflected in this paper. Though limitations, including how to best use definitions for identity versus diagnostic criteria, are still being discussed and debated. Hence, though the term NDD was used according to the DMS-5 criteria exclusively here, we recognize there is ongoing debate within the community about the extent to which this term should be used to represent all individuals with a variation in neurodevelopment and/or cognitive parameters.

Supplemental Figures

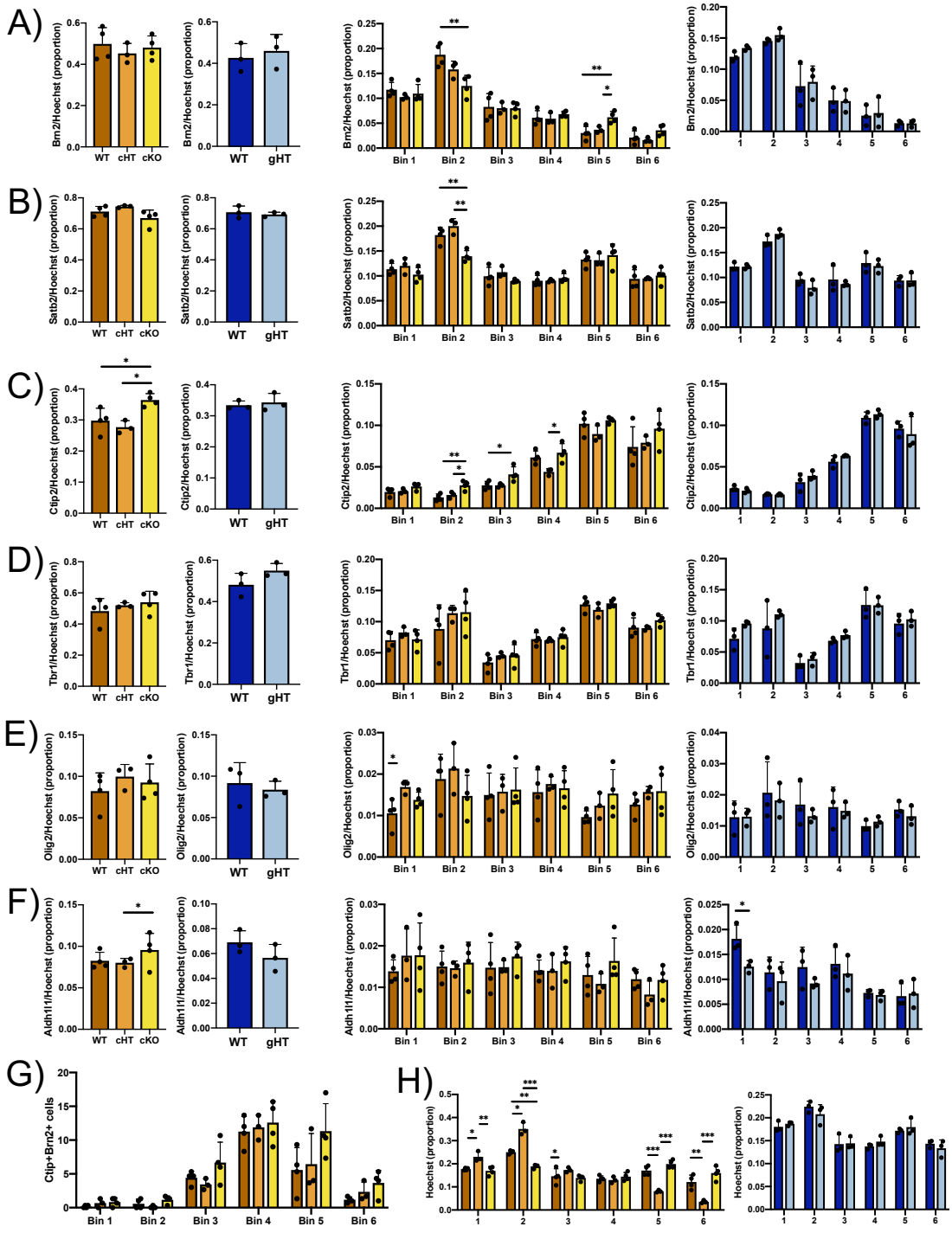

Supplementary Figure 1. Proportion of neural cells in *Chd4* cHT, cKO and gHT mouse models. A-G) Proportion of Brn2 (A), Satb2 (B), Ctip2 (C), Tbr1 (D), Olig2 (E), Aldh1l1 (F), and Ctip2 Brn2

double positive cells (G) over Hoechst in the somatosensory cortex of *Chd4* cHT, cKO, and gHT mouse models and respective controls. Total proportion (left) and proportion per bin (right) are shown. **H)** Proportion of Hoechst cells in each bin over total Hoechst in *Chd4* cHT, cKO, and gHT mouse models and respective controls. All statistical analyses are via One-way ANOVA with Tukey's post-hoc test (*Emx1-Cre line*) or unpaired Student's t-test (*CMV-Cre line*). * $p < 0.05$. ** $p < 0.01$. Biological n = 4 (WT-*Emx1*), 3 (cHT), 4 (cKO), 3 (WT-*CMV*), and 3 (gHT).

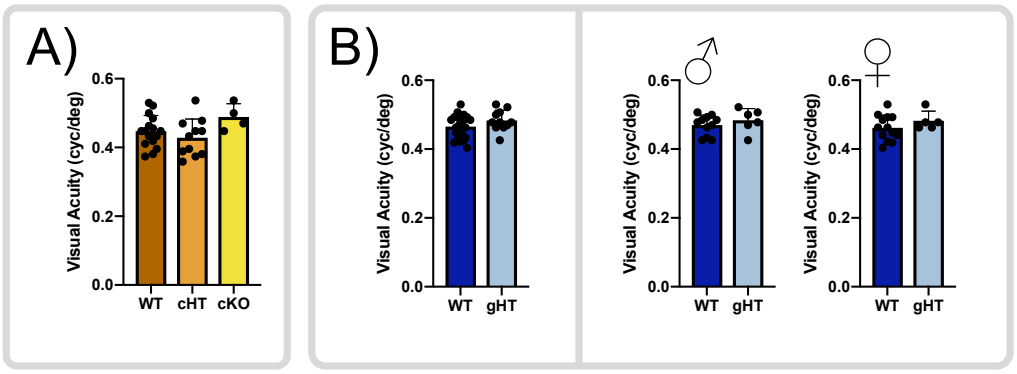

Supplementary Figure 2. Visual acuity is unchanged in *Chd4* cHT, cKO and female gHT mouse models. A) Visual acuity of WT, *Chd4* cHT and *Chd4* cKO mice. **B)** Visual acuity of total (left) and male and female (right) WT and *Chd4* gHT mice.

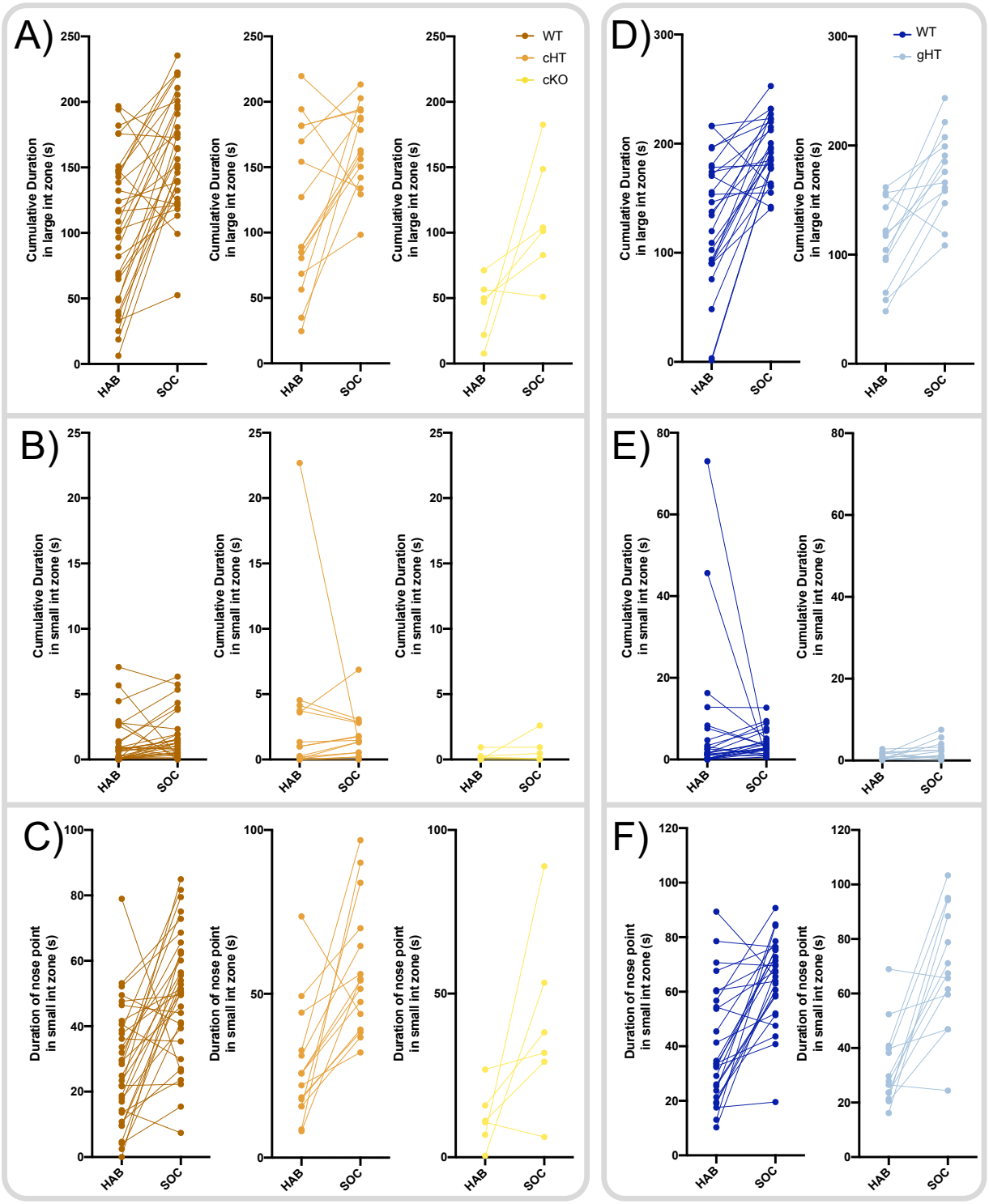

Supplementary Figure 3. Individual mouse data in adult social interaction test of *Chd4* cHT, cKO and gHT mouse models. A) Total cumulative duration WT (left), *Chd4* cHT (middle) and *Chd4* cKO (right) mice spend in the large interaction zone during habituation (HAB) and social (SOC) trials. **B)**

Total cumulative duration WT (left), *Chd4* cHT (middle) and *Chd4* cKO (right) spend in the small interaction zone during habituation and social trials. **C)** Total cumulative duration the noses of WT (left), *Chd4* cHT (middle) and *Chd4* cKO (right) spend in the small interaction zone during habituation and social trials. **D)** Total cumulative duration WT (left) and *Chd4* cHT (right) mice spend in the large interaction zone during habituation and social trials. **E)** Total cumulative duration WT (left) and *Chd4* cHT (right) spend in the small interaction zone during habituation and social trials. **F)** Total cumulative duration the noses of WT (left) and *Chd4* cHT (right) spend in the small interaction zone during habituation and social trials. Biological n = 32 (WT-*Emx1*, 19♂: 13♀), 15 (cHT, 9♂: 6♀), 6 (cKO, 3♂: 3♀), 26 (WT-*CMV*, 13♂: 13♀), and 13 (gHT, 8♂: 5♀).

References

1. Francés L, Quintero J, Fernández A, et al. Current state of knowledge on the prevalence of neurodevelopmental disorders in childhood according to the DSM-5: a systematic review in accordance with the PRISMA criteria. *Child Adolesc Psychiatry Ment Health*. Mar 31 2022;16(1):27. doi:10.1186/s13034-022-00462-1
2. Canada PHAo. Infographic: Developmental Disabilities or Disorders in Canada - Highlights from the 2017 Canadian Survey on Disability. 2023.
3. Zwaigenbaum L, Penner M. Autism spectrum disorder: advances in diagnosis and evaluation. *BMJ*. May 21 2018;361:k1674. doi:10.1136/bmj.k1674
4. Zwaigenbaum L, Bishop S, Stone WL, et al. Rethinking autism spectrum disorder assessment for children during COVID-19 and beyond. *Autism Res*. Nov 2021;14(11):2251-2259. doi:10.1002/aur.2615
5. Daniels AM, Mandell DS. Explaining differences in age at autism spectrum disorder diagnosis: a critical review. *Autism*. Jul 2014;18(5):583-97. doi:10.1177/1362361313480277
6. Kita Y, Ashizawa F, Inagaki M. Prevalence estimates of neurodevelopmental disorders in Japan: A community sample questionnaire study. *Psychiatry Clin Neurosci*. Feb 2020;74(2):118-123. doi:10.1111/pcn.12950
7. Bargiela S, Steward R, Mandy W. The Experiences of Late-diagnosed Women with Autism Spectrum Conditions: An Investigation of the Female Autism Phenotype. *J Autism Dev Disord*. Oct 2016;46(10):3281-94. doi:10.1007/s10803-016-2872-8
8. Lai MC, Lombardo MV, Chakrabarti B, et al. Neural self-representation in autistic women and association with 'compensatory camouflaging'. *Autism*. Jul 2019;23(5):1210-1223. doi:10.1177/1362361318807159
9. Lai MC, Lombardo MV, Ruigrok AN, et al. Quantifying and exploring camouflaging in men and women with autism. *Autism*. Aug 2017;21(6):690-702. doi:10.1177/1362361316671012
10. Simonoff E, Pickles A, Charman T, Chandler S, Loucas T, Baird G. Psychiatric disorders in children with autism spectrum disorders: prevalence, comorbidity, and associated factors in a population-derived sample. *J Am Acad Child Adolesc Psychiatry*. Aug 2008;47(8):921-9. doi:10.1097/CHI.0b013e318179964f
11. Muskens JB, Velders FP, Staal WG. Medical comorbidities in children and adolescents with autism spectrum disorders and attention deficit hyperactivity disorders: a systematic review. *Eur Child Adolesc Psychiatry*. Sep 2017;26(9):1093-1103. doi:10.1007/s00787-017-1020-0
12. Bourgeron T. What Do We Know about Early Onset Neurodevelopmental Disorders? : MIT Press, Cambridge (MA); 2015.
13. Peter H. *First years of human chromosomes: the beginnings of human cytogenetics* . Scion Publishing Ltd; 2006.
14. Garber KB, Visootsak J, Warren ST. Fragile X syndrome. *Eur J Hum Genet*. Jun 2008;16(6):666-72. doi:10.1038/ejhg.2008.61
15. Yamamoto T. Genomic Aberrations Associated with the Pathophysiological Mechanisms of Neurodevelopmental Disorders. *Cells*. Sep 04 2021;10(9)doi:10.3390/cells10092317
16. Cooper GM, Coe BP, Girirajan S, et al. A copy number variation morbidity map of developmental delay. *Nat Genet*. Aug 14 2011;43(9):838-46. doi:10.1038/ng.909
17. Kaminsky EB, Kaul V, Paschall J, et al. An evidence-based approach to establish the functional and clinical significance of copy number variants in intellectual and developmental disabilities. *Genet Med*. Sep 2011;13(9):777-84. doi:10.1097/GIM.0b013e31822c79f9
18. Ropers HH. Genetics of early onset cognitive impairment. *Annu Rev Genomics Hum Genet*. 2010;11:161-87. doi:10.1146/annurev-genom-082509-141640
19. Kochinke K, Zweier C, Nijhof B, et al. Systematic Phenomics Analysis Deconvolutes Genes Mutated in Intellectual Disability into Biologically Coherent Modules. *Am J Hum Genet*. Jan 2016;98(1):149-64. doi:10.1016/j.ajhg.2015.11.024

20. Hsueh YP. Synaptic Formation, Neural Circuits and Neurodevelopmental Disorders Controlled by Signaling, Translation, and Epigenetic Regulation. *Dev Neurobiol*. 01 2019;79(1):2-7. doi:10.1002/dneu.22655
21. De Rubeis S, He X, Goldberg AP, et al. Synaptic, transcriptional and chromatin genes disrupted in autism. *Nature*. Nov 2014;515(7526):209-15. doi:10.1038/nature13772
22. Study DDD. Prevalence and architecture of de novo mutations in developmental disorders. *Nature*. 02 2017;542(7642):433-438. doi:10.1038/nature21062
23. Iossifov I, O'Roak BJ, Sanders SJ, et al. The contribution of de novo coding mutations to autism spectrum disorder. *Nature*. Nov 2014;515(7526):216-21. doi:10.1038/nature13908
24. Neale BM, Kou Y, Liu L, et al. Patterns and rates of exonic de novo mutations in autism spectrum disorders. *Nature*. Apr 2012;485(7397):242-5. doi:10.1038/nature11011
25. O'Roak BJ, Vives L, Girirajan S, et al. Sporadic autism exomes reveal a highly interconnected protein network of de novo mutations. *Nature*. Apr 2012;485(7397):246-50. doi:10.1038/nature10989
26. Zahir FR, Brown CJ. Epigenetic impacts on neurodevelopment: pathophysiological mechanisms and genetic modes of action. *Pediatr Res*. May 2011;69(5 Pt 2):92R-100R. doi:10.1203/PDR.0b013e318213565e
27. Goodwin LR, Picketts DJ. The role of ISWI chromatin remodeling complexes in brain development and neurodevelopmental disorders. *Mol Cell Neurosci*. 03 2018;87:55-64. doi:10.1016/j.mcn.2017.10.008
28. Yuen RK, Merico D, Cao H, et al. Genome-wide characteristics of de novo mutations in autism. *NPJ Genom Med*. Aug 2016;1:160271-1602710. doi:10.1038/npjgenmed.2016.27
29. Iwase S, Bérubé NG, Zhou Z, et al. Epigenetic Etiology of Intellectual Disability. *J Neurosci*. 11 2017;37(45):10773-10782. doi:10.1523/JNEUROSCI.1840-17.2017
30. Franklin TB, Mansuy IM. The involvement of epigenetic defects in mental retardation. *Neurobiol Learn Mem*. Jul 2011;96(1):61-7. doi:10.1016/j.nlm.2011.04.001
31. van Bokhoven H, Kramer JM. Disruption of the epigenetic code: an emerging mechanism in mental retardation. *Neurobiol Dis*. Jul 2010;39(1):3-12. doi:10.1016/j.nbd.2010.03.010
32. Kramer JM, van Bokhoven H. Genetic and epigenetic defects in mental retardation. *Int J Biochem Cell Biol*. Jan 2009;41(1):96-107. doi:10.1016/j.biocel.2008.08.009
33. Coe BP, Girirajan S, Eichler EE. A genetic model for neurodevelopmental disease. *Curr Opin Neurobiol*. Oct 2012;22(5):829-36. doi:10.1016/j.conb.2012.04.007
34. Posthuma D, Polderman TJ. What have we learned from recent twin studies about the etiology of neurodevelopmental disorders? *Curr Opin Neurol*. Apr 2013;26(2):111-21. doi:10.1097/WCO.0b013e32835f19c3
35. Kirov G, Pocklington AJ, Holmans P, et al. De novo CNV analysis implicates specific abnormalities of postsynaptic signalling complexes in the pathogenesis of schizophrenia. *Mol Psychiatry*. Feb 2012;17(2):142-53. doi:10.1038/mp.2011.154
36. Gilman SR, Iossifov I, Levy D, Ronemus M, Wigler M, Vitkup D. Rare de novo variants associated with autism implicate a large functional network of genes involved in formation and function of synapses. *Neuron*. Jun 09 2011;70(5):898-907. doi:10.1016/j.neuron.2011.05.021
37. O'Roak BJ, Vives L, Fu W, et al. Multiplex targeted sequencing identifies recurrently mutated genes in autism spectrum disorders. *Science*. Dec 2012;338(6114):1619-22. doi:10.1126/science.1227764
38. van Holde K, Zlatanova J. Chromatin fiber structure: Where is the problem now? *Semin Cell Dev Biol*. Oct 2007;18(5):651-8. doi:10.1016/j.semcdb.2007.08.005
39. Clapier CR, Iwasa J, Cairns BR, Peterson CL. Mechanisms of action and regulation of ATP-dependent chromatin-remodelling complexes. *Nat Rev Mol Cell Biol*. 07 2017;18(7):407-422. doi:10.1038/nrm.2017.26
40. Tyagi M, Imam N, Verma K, Patel AK. Chromatin remodelers: We are the drivers!! *Nucleus*. Jul 03 2016;7(4):388-404. doi:10.1080/19491034.2016.1211217

41. Timpano S, Picketts DJ. Neurodevelopmental Disorders Caused by Defective Chromatin Remodeling: Phenotypic Complexity Is Highlighted by a Review of ATRX Function. *Front Genet*. 2020;11:885. doi:10.3389/fgene.2020.00885
42. Zhong Y, Paudel BP, Ryan DP, et al. CHD4 slides nucleosomes by decoupling entry- and exit-side DNA translocation. *Nat Commun*. Mar 23 2020;11(1):1519. doi:10.1038/s41467-020-15183-2
43. Zhu YS, Zhu J. Molecular and cellular functions of long non-coding RNAs in prostate and breast cancer. *Adv Clin Chem*. 2022;106:91-179. doi:10.1016/bs.acc.2021.09.005
44. Li W, Mills AA. Architects of the genome: CHD dysfunction in cancer, developmental disorders and neurological syndromes. *Epigenomics*. 2014;6(4):381-95. doi:10.2217/epi.14.31
45. Delmas V, Stokes DG, Perry RP. A mammalian DNA-binding protein that contains a chromodomain and an SNF2/SWI2-like helicase domain. *Proc Natl Acad Sci U S A*. Mar 15 1993;90(6):2414-8. doi:10.1073/pnas.90.6.2414
46. Musselman CA, Ramírez J, Sims JK, et al. Bivalent recognition of nucleosomes by the tandem PHD fingers of the CHD4 ATPase is required for CHD4-mediated repression. *Proc Natl Acad Sci U S A*. Jan 17 2012;109(3):787-92. doi:10.1073/pnas.1113655109
47. Watson AA, Mahajan P, Mertens HD, et al. The PHD and chromo domains regulate the ATPase activity of the human chromatin remodeler CHD4. *J Mol Biol*. Sep 07 2012;422(1):3-17. doi:10.1016/j.jmb.2012.04.031
48. Musselman CA, Mansfield RE, Garske AL, et al. Binding of the CHD4 PHD2 finger to histone H3 is modulated by covalent modifications. *Biochem J*. Sep 25 2009;423(2):179-87. doi:10.1042/BJ20090870
49. Mansfield RE, Musselman CA, Kwan AH, et al. Plant homeodomain (PHD) fingers of CHD4 are histone H3-binding modules with preference for unmodified H3K4 and methylated H3K9. *J Biol Chem*. Apr 01 2011;286(13):11779-91. doi:10.1074/jbc.M110.208207
50. Sanchez R, Zhou MM. The PHD finger: a versatile epigenome reader. *Trends Biochem Sci*. Jul 2011;36(7):364-72. doi:10.1016/j.tibs.2011.03.005
51. Musselman CA, Kutateladze TG. Handpicking epigenetic marks with PHD fingers. *Nucleic Acids Res*. Nov 2011;39(21):9061-71. doi:10.1093/nar/gkr613
52. Hall JA, Georgel PT. CHD proteins: a diverse family with strong ties. *Biochem Cell Biol*. Aug 2007;85(4):463-76. doi:10.1139/O07-063
53. Micucci JA, Sperry ED, Martin DM. Chromodomain helicase DNA-binding proteins in stem cells and human developmental diseases. *Stem Cells Dev*. Apr 2015;24(8):917-26. doi:10.1089/scd.2014.0544
54. Pierson TM, Otero MG, Grand K, et al. The NuRD complex and macrocephaly associated neurodevelopmental disorders. *Am J Med Genet C Semin Med Genet*. 12 2019;181(4):548-556. doi:10.1002/ajmg.c.31752
55. Yasin H, Zahir FR. Chromodomain helicase DNA-binding proteins and neurodevelopmental disorders. *Journal of Translational Genetics and Genomics*. 2020;4(4):307-319.
56. Carvill GL, Heavin SB, Yendle SC, et al. Targeted resequencing in epileptic encephalopathies identifies de novo mutations in CHD2 and SYNGAP1. *Nat Genet*. Jul 2013;45(7):825-30. doi:10.1038/ng.2646
57. Suls A, Jaehn JA, Kecskés A, et al. De novo loss-of-function mutations in CHD2 cause a fever-sensitive myoclonic epileptic encephalopathy sharing features with Dravet syndrome. *Am J Hum Genet*. Nov 07 2013;93(5):967-75. doi:10.1016/j.ajhg.2013.09.017
58. Lund C, Brodtkorb E, Øye AM, Røsby O, Selmer KK. CHD2 mutations in Lennox-Gastaut syndrome. *Epilepsy Behav*. Apr 2014;33:18-21. doi:10.1016/j.yebeh.2014.02.005
59. Pilarowski GO, Vernon HJ, Applegate CD, et al. Missense variants in the chromatin remodeler CHD1 are associated with neurodevelopmental disability. *J Med Genet*. Aug 2018;55(8):561-566. doi:10.1136/jmedgenet-2017-104759
60. Snijders Blok L, Rousseau J, Twist J, et al. CHD3 helicase domain mutations cause a neurodevelopmental syndrome with macrocephaly and impaired speech and language. *Nat Commun*. 11 2018;9(1):4619. doi:10.1038/s41467-018-06014-6

61. Sifrim A, Hitz MP, Wilsdon A, et al. Distinct genetic architectures for syndromic and nonsyndromic congenital heart defects identified by exome sequencing. *Nat Genet*. 09 2016;48(9):1060-5. doi:10.1038/ng.3627
62. Weiss K, Lazar HP, Kurolap A, et al. The CHD4-related syndrome: a comprehensive investigation of the clinical spectrum, genotype-phenotype correlations, and molecular basis. *Genet Med*. 02 2020;22(2):389-397. doi:10.1038/s41436-019-0612-0
63. Weiss K, Terhal PA, Cohen L, et al. De Novo Mutations in CHD4, an ATP-Dependent Chromatin Remodeler Gene, Cause an Intellectual Disability Syndrome with Distinctive Dysmorphisms. *Am J Hum Genet*. Oct 2016;99(4):934-941. doi:10.1016/j.ajhg.2016.08.001
64. Laut AK, Dorneburg C, Fürstberger A, et al. CHD5 inhibits metastasis of neuroblastoma. *Oncogene*. Jan 2022;41(5):622-633. doi:10.1038/s41388-021-02081-0
65. Parenti I, Lehalle D, Nava C, et al. Missense and truncating variants in CHD5 in a dominant neurodevelopmental disorder with intellectual disability, behavioral disturbances, and epilepsy. *Hum Genet*. Jul 2021;140(7):1109-1120. doi:10.1007/s00439-021-02283-2
66. Bergman JE, Janssen N, Hoefsloot LH, Jongmans MC, Hofstra RM, van Ravenswaaij-Arts CM. CHD7 mutations and CHARGE syndrome: the clinical implications of an expanding phenotype. *J Med Genet*. May 2011;48(5):334-42. doi:10.1136/jmg.2010.087106
67. de Arriba Muñoz A, Monge Galindo L, López Pisón J, et al. CHARGE syndrome and CHD7 gene mutation. *Neurologia*. May 2011;26(4):255. doi:10.1016/j.nrl.2010.10.011
68. Wincent J, Holmberg E, Strömland K, et al. CHD7 mutation spectrum in 28 Swedish patients diagnosed with CHARGE syndrome. *Clin Genet*. Jul 2008;74(1):31-8. doi:10.1111/j.1399-0004.2008.01014.x
69. Jiang YH, Yuen RK, Jin X, et al. Detection of clinically relevant genetic variants in autism spectrum disorder by whole-genome sequencing. *Am J Hum Genet*. Aug 08 2013;93(2):249-63. doi:10.1016/j.ajhg.2013.06.012
70. Thomas AT, Waite J, Williams CA, Kirk J, Oliver C, Richards C. Phenotypic characteristics and variability in CHARGE syndrome: a PRISMA compliant systematic review and meta-analysis. *J Neurodev Disord*. Aug 31 2022;14(1):49. doi:10.1186/s11689-022-09459-5
71. Yasin H, Gibson WT, Langlois S, et al. A distinct neurodevelopmental syndrome with intellectual disability, autism spectrum disorder, characteristic facies, and macrocephaly is caused by defects in CHD8. *J Hum Genet*. Apr 2019;64(4):271-280. doi:10.1038/s10038-019-0561-0
72. Talkowski ME, Rosenfeld JA, Blumenthal I, et al. Sequencing chromosomal abnormalities reveals neurodevelopmental loci that confer risk across diagnostic boundaries. *Cell*. Apr 2012;149(3):525-37. doi:10.1016/j.cell.2012.03.028
73. McCarthy SE, Gillis J, Kramer M, et al. De novo mutations in schizophrenia implicate chromatin remodeling and support a genetic overlap with autism and intellectual disability. *Mol Psychiatry*. Jun 2014;19(6):652-8. doi:10.1038/mp.2014.29
74. Pinto D, Delaby E, Merico D, et al. Convergence of genes and cellular pathways dysregulated in autism spectrum disorders. *Am J Hum Genet*. May 01 2014;94(5):677-94. doi:10.1016/j.ajhg.2014.03.018
75. Capelli LP, Krepischi AC, Gurgel-Giannetti J, et al. Deletion of the RMGA and CHD2 genes in a child with epilepsy and mental deficiency. *Eur J Med Genet*. Feb 2012;55(2):132-4. doi:10.1016/j.ejmg.2011.10.004
76. Rauch A, Wieczorek D, Graf E, et al. Range of genetic mutations associated with severe non-syndromic sporadic intellectual disability: an exome sequencing study. *Lancet*. Nov 10 2012;380(9854):1674-82. doi:10.1016/S0140-6736(12)61480-9
77. Yamada K, Fukushi D, Ono T, et al. Characterization of a de novo balanced t(4;20)(q33;q12) translocation in a patient with mental retardation. *Am J Med Genet A*. Dec 2010;152A(12):3057-67. doi:10.1002/ajmg.a.33174
78. Vera G, Sorlin A, Delplancq G, et al. Clinical and molecular description of 19 patients with GATAD2B-Associated Neurodevelopmental Disorder (GAND). *Eur J Med Genet*. Oct 2020;63(10):104004. doi:10.1016/j.ejmg.2020.104004

79. Cukier HN, Rabionet R, Konidari I, et al. Novel variants identified in methyl-CpG-binding domain genes in autistic individuals. *Neurogenetics*. Jul 2010;11(3):291-303. doi:10.1007/s10048-009-0228-7
80. Jones PL, Veenstra GJ, Wade PA, et al. Methylated DNA and MeCP2 recruit histone deacetylase to repress transcription. *Nat Genet*. Jun 1998;19(2):187-91. doi:10.1038/561
81. Wade PA, Gegonne A, Jones PL, Ballestar E, Aubry F, Wolffe AP. Mi-2 complex couples DNA methylation to chromatin remodelling and histone deacetylation. *Nat Genet*. Sep 1999;23(1):62-6. doi:10.1038/12664
82. Xue Y, Wong J, Moreno GT, Young MK, Côté J, Wang W. NURD, a novel complex with both ATP-dependent chromatin-remodeling and histone deacetylase activities. *Mol Cell*. Dec 1998;2(6):851-61. doi:10.1016/s1097-2765(00)80299-3
83. Zhang Y, LeRoy G, Seelig HP, Lane WS, Reinberg D. The dermatomyositis-specific autoantigen Mi2 is a component of a complex containing histone deacetylase and nucleosome remodeling activities. *Cell*. Oct 16 1998;95(2):279-89. doi:10.1016/s0092-8674(00)81758-4
84. Nitarska J, Smith JG, Sherlock WT, et al. A Functional Switch of NuRD Chromatin Remodeling Complex Subunits Regulates Mouse Cortical Development. *Cell Rep*. 11 2016;17(6):1683-1698. doi:10.1016/j.celrep.2016.10.022
85. Dos Santos RL, Tosti L, Radzisheuskaya A, et al. MBD3/NuRD Facilitates Induction of Pluripotency in a Context-Dependent Manner. *Cell Stem Cell*. Sep 04 2014;15(3):392. doi:10.1016/j.stem.2014.08.005
86. Kaji K, Nichols J, Hendrich B. Mbd3, a component of the NuRD co-repressor complex, is required for development of pluripotent cells. *Development*. Mar 2007;134(6):1123-32. doi:10.1242/dev.02802
87. Fujita N, Jaye DL, Geigerman C, et al. MTA3 and the Mi-2/NuRD complex regulate cell fate during B lymphocyte differentiation. *Cell*. Oct 01 2004;119(1):75-86. doi:10.1016/j.cell.2004.09.014
88. Yildirim O, Li R, Hung JH, et al. Mbd3/NURD complex regulates expression of 5-hydroxymethylcytosine marked genes in embryonic stem cells. *Cell*. Dec 23 2011;147(7):1498-510. doi:10.1016/j.cell.2011.11.054
89. Bornelöv S, Reynolds N, Xenophontos M, et al. The Nucleosome Remodeling and Deacetylation Complex Modulates Chromatin Structure at Sites of Active Transcription to Fine-Tune Gene Expression. *Mol Cell*. Jul 05 2018;71(1):56-72.e4. doi:10.1016/j.molcel.2018.06.003
90. Larrigan S, Shah S, Fernandes A, Mattar P. Chromatin Remodeling in the Brain-a NuRDevelopmental Odyssey. *Int J Mol Sci*. Apr 30 2021;22(9)doi:10.3390/ijms22094768
91. Low JKK, Silva APG, Sharifi Tabar M, et al. The Nucleosome Remodeling and Deacetylase Complex Has an Asymmetric, Dynamic, and Modular Architecture. *Cell Rep*. Dec 01 2020;33(9):108450. doi:10.1016/j.celrep.2020.108450
92. Millard CJ, Fairall L, Ragan TJ, Savva CG, Schwabe JWR. The topology of chromatin-binding domains in the NuRD deacetylase complex. *Nucleic Acids Res*. Dec 16 2020;48(22):12972-12982. doi:10.1093/nar/gkaa1121
93. Millard CJ, Varma N, Saleh A, et al. The structure of the core NuRD repression complex provides insights into its interaction with chromatin. *Elife*. Apr 21 2016;5:e13941. doi:10.7554/eLife.13941
94. Zhang W, Aubert A, Gomez de Segura JM, et al. The Nucleosome Remodeling and Deacetylase Complex NuRD Is Built from Preformed Catalytically Active Sub-modules. *J Mol Biol*. Jul 17 2016;428(14):2931-42. doi:10.1016/j.jmb.2016.04.025
95. Zhang J, Jackson AF, Naito T, et al. Harnessing of the nucleosome-remodeling-deacetylase complex controls lymphocyte development and prevents leukemogenesis. *Nat Immunol*. Nov 2011;13(1):86-94. doi:10.1038/ni.2150
96. Topark-Ngarm A, Golonzhka O, Peterson VJ, et al. CTIP2 associates with the NuRD complex on the promoter of p57KIP2, a newly identified CTIP2 target gene. *J Biol Chem*. Oct 2006;281(43):32272-83. doi:10.1074/jbc.M602776200

97. Cismasiu VB, Adamo K, Gecewicz J, Duque J, Lin Q, Avram D. BCL11B functionally associates with the NuRD complex in T lymphocytes to repress targeted promoter. *Oncogene*. Oct 2005;24(45):6753-64. doi:10.1038/sj.onc.1208904
98. Sridharan R, Smale ST. Predominant interaction of both Ikaros and Helios with the NuRD complex in immature thymocytes. *J Biol Chem*. Oct 12 2007;282(41):30227-38. doi:10.1074/jbc.M702541200
99. Hoffmeister H, Fuchs A, Erdel F, et al. CHD3 and CHD4 form distinct NuRD complexes with different yet overlapping functionality. *Nucleic Acids Res*. Oct 13 2017;45(18):10534-10554. doi:10.1093/nar/gkx711
100. Wang T, Hoekzema K, Vecchio D, et al. Large-scale targeted sequencing identifies risk genes for neurodevelopmental disorders. *Nat Commun*. Oct 01 2020;11(1):4932. doi:10.1038/s41467-020-18723-y
101. Coe BP, Stessman HAF, Sulovari A, et al. Neurodevelopmental disease genes implicated by de novo mutation and copy number variation morbidity. *Nat Genet*. Jan 2019;51(1):106-116. doi:10.1038/s41588-018-0288-4
102. Ostapcuk V, Mohn F, Carl SH, et al. Activity-dependent neuroprotective protein recruits HP1 and CHD4 to control lineage-specifying genes. *Nature*. May 2018;557(7707):739-743. doi:10.1038/s41586-018-0153-8
103. Sharifi Tabar M, Giardina C, Feng Y, et al. Unique protein interaction networks define the chromatin remodelling module of the NuRD complex. *FEBS J*. Jan 2022;289(1):199-214. doi:10.1111/febs.16112
104. Helsmoortel C, Vulto-van Silfhout AT, Coe BP, et al. A SWI/SNF-related autism syndrome caused by de novo mutations in ADNP. *Nat Genet*. Apr 2014;46(4):380-4. doi:10.1038/ng.2899
105. Gupta A, Tsai LH, Wynshaw-Boris A. Life is a journey: a genetic look at neocortical development. *Nat Rev Genet*. May 2002;3(5):342-55. doi:10.1038/nrg799
106. Kwan KY, Sestan N, Anton ES. Transcriptional co-regulation of neuronal migration and laminar identity in the neocortex. *Development*. May 2012;139(9):1535-46. doi:10.1242/dev.069963
107. Miller FD, Gauthier AS. Timing is everything: making neurons versus glia in the developing cortex. *Neuron*. May 03 2007;54(3):357-69. doi:10.1016/j.neuron.2007.04.019
108. O'Shaughnessy-Kirwan A, Signolet J, Costello I, Gharbi S, Hendrich B. Constraint of gene expression by the chromatin remodelling protein CHD4 facilitates lineage specification. *Development*. Aug 01 2015;142(15):2586-97. doi:10.1242/dev.125450
109. Sparmann A, Xie Y, Verhoeven E, et al. The chromodomain helicase Chd4 is required for Polycomb-mediated inhibition of astroglial differentiation. *EMBO J*. May 2013;32(11):1598-612. doi:10.1038/emboj.2013.93
110. Yamada T, Yang Y, Hemberg M, et al. Promoter decommissioning by the NuRD chromatin remodeling complex triggers synaptic connectivity in the mammalian brain. *Neuron*. Jul 2014;83(1):122-34. doi:10.1016/j.neuron.2014.05.039
111. Yang Y, Yamada T, Hill KK, et al. Chromatin remodeling inactivates activity genes and regulates neural coding. *Science*. Jul 2016;353(6296):300-305. doi:10.1126/science.aad4225
112. Goodman JV, Yamada T, Yang Y, et al. The chromatin remodeling enzyme Chd4 regulates genome architecture in the mouse brain. *Nat Commun*. Jul 2020;11(1):3419. doi:10.1038/s41467-020-17065-z
113. Williams CJ, Naito T, Arco PG, et al. The chromatin remodeler Mi-2beta is required for CD4 expression and T cell development. *Immunity*. Jun 2004;20(6):719-33. doi:10.1016/j.immuni.2004.05.005
114. Dahlstrand J, Lardelli M, Lendahl U. Nestin mRNA expression correlates with the central nervous system progenitor cell state in many, but not all, regions of developing central nervous system. *Brain Res Dev Brain Res*. Jan 14 1995;84(1):109-29. doi:10.1016/0165-3806(94)00162-s
115. Gorski JA, Talley T, Qiu M, Puelles L, Rubenstein JL, Jones KR. Cortical excitatory neurons and glia, but not GABAergic neurons, are produced in the Emx1-expressing lineage. *J Neurosci*. Aug 2002;22(15):6309-14. doi:20026564

116. Shibata S, Kashiwagi M, Morgan BA, Georgopoulos K. Functional interactions between Mi-2β and AP1 complexes control response and recovery from skin barrier disruption. *J Exp Med*. Mar 02 2020;217(3)doi:10.1084/jem.20182402
117. Albani SH, Andrawis MM, Abella RJ, Fulghum JT, Vafamand N, Dumas TC. Behavior in the elevated plus maze is differentially affected by testing conditions in rats under and over three weeks of age. *Front Behav Neurosci*. 2015;9:31. doi:10.3389/fnbeh.2015.00031
118. Knock E, Pereira J, Lombard PD, et al. The methyl binding domain 3/nucleosome remodelling and deacetylase complex regulates neural cell fate determination and terminal differentiation in the cerebral cortex. *Neural Dev*. May 02 2015;10:13. doi:10.1186/s13064-015-0040-z
119. Herbert MR, Ziegler DA, Deutsch CK, et al. Dissociations of cerebral cortex, subcortical and cerebral white matter volumes in autistic boys. *Brain*. May 2003;126(Pt 5):1182-92. doi:10.1093/brain/awg110
120. Zhao Y, Yang L, Gong G, Cao Q, Liu J. Identify aberrant white matter microstructure in ASD, ADHD and other neurodevelopmental disorders: A meta-analysis of diffusion tensor imaging studies. *Prog Neuropsychopharmacol Biol Psychiatry*. Mar 08 2022;113:110477. doi:10.1016/j.pnpbp.2021.110477
121. Xu R, Brawner AT, Li S, et al. OLIG2 Drives Abnormal Neurodevelopmental Phenotypes in Human iPSC-Based Organoid and Chimeric Mouse Models of Down Syndrome. *Cell Stem Cell*. Jun 06 2019;24(6):908-926.e8. doi:10.1016/j.stem.2019.04.014
122. Chakrabarti L, Best TK, Cramer NP, et al. Olig1 and Olig2 triplication causes developmental brain defects in Down syndrome. *Nat Neurosci*. Aug 2010;13(8):927-34. doi:10.1038/nn.2600
123. Lu J, Lian G, Zhou H, et al. OLIG2 over-expression impairs proliferation of human Down syndrome neural progenitors. *Hum Mol Genet*. May 15 2012;21(10):2330-40. doi:10.1093/hmg/dds052
124. Liu W, Zhou H, Liu L, et al. Disruption of neurogenesis and cortical development in transgenic mice misexpressing Olig2, a gene in the Down syndrome critical region. *Neurobiol Dis*. May 2015;77:106-16. doi:10.1016/j.nbd.2015.02.021
125. Szu J, Wojcinski A, Jiang P, Kesari S. Impact of the Olig Family on Neurodevelopmental Disorders. *Front Neurosci*. 2021;15:659601. doi:10.3389/fnins.2021.659601
126. Vissers LE, van Ravenswaaij CM, Admiraal R, et al. Mutations in a new member of the chromodomain gene family cause CHARGE syndrome. *Nat Genet*. Sep 2004;36(9):955-7. doi:10.1038/ng1407
127. Chénier S, Yoon G, Argiropoulos B, et al. CHD2 haploinsufficiency is associated with developmental delay, intellectual disability, epilepsy and neurobehavioural problems. *J Neurodev Disord*. 2014;6(1):9. doi:10.1186/1866-1955-6-9
128. Jiménez JA, Ptacek TS, Tuttle AH, et al. Chd8 haploinsufficiency impairs early brain development and protein homeostasis later in life. *Mol Autism*. Oct 05 2020;11(1):74. doi:10.1186/s13229-020-00369-8
129. Sankaran VG, Menne TF, Xu J, et al. Human fetal hemoglobin expression is regulated by the developmental stage-specific repressor BCL11A. *Science*. Dec 2008;322(5909):1839-42. doi:10.1126/science.1165409
130. Arlotta P, Molyneaux BJ, Jabaudon D, Yoshida Y, Macklis JD. Ctip2 controls the differentiation of medium spiny neurons and the establishment of the cellular architecture of the striatum. *J Neurosci*. Jan 16 2008;28(3):622-32. doi:10.1523/JNEUROSCI.2986-07.2008
131. Burnett LE, Koppensteiner P, Symonova O, et al. Subcortical circuit dysfunctions delay perceptual decision-making in autism models. *bioRxiv*. 2022:2022.10.11.511691. doi:10.1101/2022.10.11.511691
132. Sen P, Sherwin E, Sandhu K, et al. The live biotherapeutic Blautia stercoris MRx0006 attenuates social deficits, repetitive behaviour, and anxiety-like behaviour in a mouse model relevant to autism. *Brain Behav Immun*. Nov 2022;106:115-126. doi:10.1016/j.bbi.2022.08.007

133. Lee B, Lee K, Panda S, et al. Nanoparticle delivery of CRISPR into the brain rescues a mouse model of fragile X syndrome from exaggerated repetitive behaviours. *Nat Biomed Eng*. Jul 2018;2(7):497-507. doi:10.1038/s41551-018-0252-8
134. Belichenko PV, Kleschevnikov AM, Becker A, et al. Down Syndrome Cognitive Phenotypes Modeled in Mice Trisomic for All HSA 21 Homologues. *PLoS One*. 2015;10(7):e0134861. doi:10.1371/journal.pone.0134861
135. Xu J, Marshall JJ, Kraniotis S, Nomura T, Zhu Y, Contractor A. Genetic disruption of Grm5 causes complex alterations in motor activity, anxiety and social behaviors. *Behav Brain Res*. Aug 06 2021;411:113378. doi:10.1016/j.bbr.2021.113378
136. Pasciuto E, Borrie SC, Kanellopoulos AK, et al. Autism Spectrum Disorders: Translating human deficits into mouse behavior. *Neurobiol Learn Mem*. Oct 2015;124:71-87. doi:10.1016/j.nlm.2015.07.013
137. Mao JH, Langley SA, Huang Y, et al. Identification of genetic factors that modify motor performance and body weight using Collaborative Cross mice. *Sci Rep*. Nov 09 2015;5:16247. doi:10.1038/srep16247
138. Masuda F, Nakajima S, Miyazaki T, et al. Motor cortex excitability and inhibitory imbalance in autism spectrum disorder assessed with transcranial magnetic stimulation: a systematic review. *Transl Psychiatry*. Mar 07 2019;9(1):110. doi:10.1038/s41398-019-0444-3
139. Safari S, Ahmadi N, Mohammadkhani R, et al. Sex differences in spatial learning and memory and hippocampal long-term potentiation at perforant pathway-dentate gyrus (PP-DG) synapses in Wistar rats. *Behav Brain Funct*. Nov 01 2021;17(1):9. doi:10.1186/s12993-021-00184-y
140. Roof RL, Zhang Q, Glasier MM, Stein DG. Gender-specific impairment on Morris water maze task after entorhinal cortex lesion. *Behav Brain Res*. Oct 21 1993;57(1):47-51. doi:10.1016/0166-4328(93)90060-4
141. Knoll A, Tabbaa M, Levitt P. Mouse population genetics phenocopies heterogeneity of human Chd8 haploinsufficiency. *bioRxiv*. 2022:2022.08. 26.504147.
142. Pinard A, Guey S, Guo D, et al. The pleiotropy associated with de novo variants in CHD4, CNOT3, and SETD5 extends to moyamoya angiopathy. *Genet Med*. Feb 2020;22(2):427-431. doi:10.1038/s41436-019-0639-2
143. Singer J. Reflections on the Neurodiversity Paradigm. 2023. https://neurodiversity2.blogspot.com/p/what.html
144. Shah PJ, Boilson M, Rutherford M, et al. Neurodevelopmental disorders and neurodiversity: definition of terms from Scotland's National Autism Implementation Team. *Br J Psychiatry*. Sep 2022;221(3):577-579. doi:10.1192/bjp.2022.43